NGR-33-010-188

# MONTE CARLO SIMULATION OF THE CLASSICAL TWO-DIMENSIONAL ONE COMPONENT PLASMA

BY

R.C. Gann*, Sudip Chakravarty†, and G.V. Chester

Laboratory of Atomic and Solid State Physics

Cornell University

Ithaca, New York 14853



## ABSTRACT

We have used Monte Carlo simulation, lattice dynamics in the harmonic approximation, and solution of the hypernetted chain equation to study the classical two-dimensional one component plasma. We find a fluid phase for $\Gamma = e^2(\pi n)^{\frac{1}{2}}/k_BT \leq 125 \pm 15$ and a solid phase for higher $\Gamma$. The solid phase shows directional long range order. In the solid phase positional long range order is lost as the thermodynamic limit is approached. We also present the results of calculation of the thermodynamic functions and one and two particle correlation functions.

# I. INTRODUCTION

This paper is concerned with the properties of a two-dimensional one component plasma. Our system consists of a single species of charged particles immersed in a uniform neutralizing background. The particles interact via a 1/r potential, where r is the two-dimensional separation. Our calculations are limited to ranges of temperature and density such that quantum effects are unimportant. We have made calculations of the equation of state in the fluid phase using both the hypernetted chain equation (HNC) and Monte Carlo simulations. Our calculations in the crystal phase were done by Monte Carlo methods.

There are two reasons why we find such a system interesting. First it can be considered as an idealized model of a bound surface layer of electrons above liquid helium four. Second there have been extensive simulations of the properties of the three-dimensional one component plasma. The extension to two dimensions may provide insight into the behavior of both systems.

We begin by briefly reviewing the state of our knowledge of the electron surface layer above liquid helium four. Several years ago Crandall and Williams[1] suggested that under favorable circumstances electrons trapped on the surface of liquid helium might crystallize to form a two-dimensional electron solid. Since in most experimental situations the density of electrons can be changed by several orders of magnitude, it was hoped that the so called Wigner crystal[2] might be within experimental reach. This led to a great deal of theoretical and experimental activity in the following years, and Chaplik[3] suggested that a similar crystallization can occur in the inversion layer near the surface of a semiconductor. In the helium context a model of a charge-compensated one component system of N electrons confined to an area A at a temperature T interacting with 1/r potential can be and has been considered as the canonical model.[4-7]

In this paper we consider only the classical behavior of the model. This is appropriate for the electron surface layer above liquid helium in the usual experimental regime. However, our model is not appropriate for the problem of the metal-oxide-silicon inversion layer where the electrons form a degenerate quantum system.

Although studies by Brown and Grimes[8] of cyclotron resonance in a tipped magnetic field have shown that the electron motion on the surface of liquid helium is two dimensional, it is clear that for a strong clamping field (most experiments require a clamping field in order to localize the electrons layer for a reasonable amount of time) one needs in principle to take into account the coupling in the perpendicular direction, for example the deformation of the helium surface.[9] However, the characteristic dimensions are such that the interelectronic spacing ( $\sim 10^4$ Å) is much larger than the spread in the charge density in the direction perpendicular to the surface ($\sim 10^2$ Å) so that the system can be considered to be essentially two-dimensional. Therefore the model of a two-dimensional electron gas, neutralized by a uniform positive background, and interacting by a $e^2/r$ potential is probably a reasonable first approximation to the experimental situation. The system is characterized by the dimensionless quantity $\Gamma = e^2/ak_BT$, where $a = (\pi n)^{\frac{1}{2}}$ and $n = N/A$.

The simulations that have been made on the three-dimensional one component plasma have established its equation of state, the phase boundary between the crystal and liquid phases, and the two particle correlation function at several densities and temperatures. In addition, Lindemann's ratio at melting has been found to be 0.17---rather close to the values for other inverse power potentials. The height of the first peak of the structure factor at freezing was found to be close to 2.85---again close to the values for other potentials. In view of these results it seemed worthwhile to carry out a similar study of the two-dimensional one component plasma. In particular we were interested in determining whether the two-dimensional system would undergo a phase transformation to a crystalline phase. To our knowledge there has not been any calculation comparing the free energies of the solid and the liquid phases which is, after all, the basic method to locate this phase transition. In this paper we present such a calculation. We employ both the hypernetted chain integral equation and the Monte Carlo technique to calculate the free energies. We have computed the thermodynamic functions and correlation functions over a wide range of $\Gamma$, $1 \leq \Gamma \leq 300$. A recent publication by Totsuji[10] contains Monte Carlo results for the thermodynamic functions and pair correlation function for $0.15 \leq \Gamma \leq 50$. Within the range of $\Gamma$ our results are generally in good agreement with those of Totsuji. On the other hand our results are quite different from a very recent computer experiment[11] which employed a special type of molecular dynamics method (PPPM: Particle-Particle/Particle-Mesh). Contrary to the $\lambda$ point transition obtained there we tentatively find a first order transition, our transition being roughly 20% higher in $\Gamma$; namely $\Gamma = 125$. Our results are qualitatively similar to the corresponding three-dimensional calculations of Hansen[12] and Pollock and Hansen[13]. We find that the triangular lattice is stable and have calculated the harmonic phonon dispersion laws for such a lattice. We also find that the two-dimensional square lattice is dynamically unstable. Our calculations for the harmonic solid are in agreement with a recent calculation by Bonsall and Maradudin[14].

Before proceeding further we should comment on the existence of two-dimensional crystalline order. Some years ago Mermin[15] published a rigorous proof, based on Bogolyubov's inequality, that two-dimensional systems cannot display long range crystalline order. The proof had two limitations. First, and probably less important, the interaction potential was assumed to fall off faster than $1/r^2$. Second, the result only applies in the thermodynamic limit. When the same mathematical methods are applied to a large but finite system one finds that no inconsistency arises from the assumption of crystalline order. Thus any system that can be studied in the laboratory or in a computer simulation can exhibit crystalline order. We do indeed find a stable crystal phase in our simulations, however,it does have unusual properties. These are described in sections VI and VII.

The plan of our paper is as follows, after formulating the problem in section II, sections III and IV are devoted to the calculations of the thermodynamic functions in the liquid and solid phases respectively. In the liquid phase we present results for both the HNC method and MC simulations. Section V is devoted to the determination of the phase boundary between the crystal and fluid phases. Lindemann's ratio and its dependence on the size of the system are discussed in section VI. The one and two particle distribution functions are presented in section VII.

## II. FORMULATION OF THE PROBLEM

Consider a system of N electrons obeying classical statistics, confined to an area A, and neutralized by a uniform positive background. The Hamiltonian, apart from the kinetic energy, which does not enter into our considerations, is then

$$H_I = \sum_{i<j} \frac{e^2}{r_{ij}} - \tfrac{1}{2}Nnv(0) \qquad (2.1)$$

where, the last term, arises from the interaction of electrons with the uniform positive background. Here $r_{ij} = |\vec{r}_i - \vec{r}_j|$ is the two-dimensional separation and $n = N/A$ is the area density of electrons. The Fourier transform of $e^2/r$ potential in two dimensions is given by

$$v(k) = e^2\int \frac{e^{i\vec{k}\cdot\vec{r}}}{r}\, d^2r = \frac{2\pi e^2}{k} \tag{2.2}$$

Once again $\vec{k} = (k_x, k_y)$ is a two-dimensional vector. For the problem of electrons bound to the surface of helium four one should use the "renormalized" charge[7]

$$\bar{e}^{\,2} = e^2[2(\varepsilon_1 + \varepsilon_2)^{-1}] \tag{2.3}$$

where we have assumed that uniform media with dielectric constants $\varepsilon_1$ and $\varepsilon_2$ fill the adjacent half spaces. The thermodynamics of this one component classical electron plasma is determined by a single dimensionless parameter,

$$\Gamma = \frac{\bar{e}^{\,2}}{k_B T a} \quad , \tag{2.4}$$

where $k_B$ is the Boltzmann constant, T the temperature and a is the average interparticle distance determined by $n = 1/(\pi a^2)$. The complete solution of the problem therefore reduces to the calculation of averages of the kind

$$\langle F\rangle = \int F(r_1 \ldots r_N) \exp\, [ - \frac{1}{k_B T} \sum_{i<j} v(r_{ij})]\, d^2r_1 \ldots d^2r_N / Q_N \tag{2.5}$$

where

$$Q_N = \int \ldots \int \exp\left[- \frac{1}{k_B T} \sum_{i<j} v(r_{ij})\right] d^2r_1 \ldots d^2r_N \quad .$$

The two particle distribution function is given by

$$P(\vec{r}_1, \vec{r}_2) = \frac{N(N-1)}{Q_N} \int \ldots \int \exp\left[ - \frac{1}{k_B T} \sum_{i<j} v(r_{ij})\right] d^2r_3 \ldots d^2r_N \ . \tag{2.6}$$

For the liquid phase $P(\vec{r}_1, \vec{r}_2) = n^2 g(r_{12})$, where $g(r)$ is the pair correlation function.

Before we proceed any further we should point out that the summation of the ring diagrams (random phase approximation) produces a divergent free energy and therefore the result analogous to Debye-Hückel limit in three dimensions does not exist. In fact it is easy to mimic the corresponding three-dimensional calculation[16,17] to obtain

$$\frac{Q_N}{N!} = N \log(1/n) + 1 + W \quad , \tag{2.7}$$



where W is the contribution of the ring diagrams

$$W = W^{2D}_{ring} = \frac{1}{4\pi n} \int_0^{q_m} q\left[\frac{2\pi n e^2}{k_B T}\,\frac{1}{q} - \log\left(1 + \left(\frac{2\pi n e^2}{k_B T}\right)\frac{1}{q}\right)\right] dq \tag{2.8}$$

which diverges as $q_m \to \infty$. This is different from the behavior of the corresponding three-dimensional integral:

$$W^{3D}_{ring} = \frac{1}{4\pi^2 n} \int_0^{\infty} q^2 \left[\left(\frac{4\pi n e^2}{k_B T}\right)\frac{1}{q^2} - \log\left(1 + \left(\frac{4\pi n e^2}{k_B T}\right)\frac{1}{q^2}\right)\right] dq \quad .$$

This high q (small r) divergence for the contribution of the ring diagrams to the energy has also been noticed by Totsuji[18]. He has, however, shown that if one includes the simplest set of next order diagrams then the divergence is cancelled. His results can be expressed as a small $\Gamma$ expansion for the excess internal energy,

$$\frac{U^{ex}}{N k_B T} = \Gamma^2(2\ell n\Gamma + 2\gamma - 1 + 2\ell n 2) + \Gamma^4[-8(\ell n\Gamma)^2 + 8(1 - 2\gamma)\ell n\Gamma + 4(1 - 2\gamma)\,\ell n 2] + \ldots \tag{2.9}$$

where $\gamma$ is Euler's constant.

## III. LIQUID PHASE CALCULATIONS

Given the pair correlation function $g(r)$ then the excess internal energy U is given by,

$$\frac{U^{ex}}{Nk_BT} = \Gamma \int_0^\infty [g(r) - 1]dr = \frac{\Gamma}{2} \int_0^\infty dk[S(k) - 1] \tag{3.1}$$

where $S(k)$ is the structure factor defined by

$$S(k) = 1 + 2 \int_0^\infty rJ_0(kr)[g(r) - 1]\,dr \tag{3.2}$$

where $J_0(x)$ is the zeroth order Bessel function. The pressure obtained from the virial theorem is

$$\frac{pA}{Nk_BT} = 1 + \frac{U^{ex}}{2Nk_BT} \quad . \tag{3.3}$$

and excess free energy is given by

$$\frac{F - F^{id}}{Nk_BT} = \int_0^\Gamma \frac{U^{ex}(\Gamma')}{Nk_BT} \frac{d\Gamma'}{\Gamma'} \tag{3.4}$$

The ideal gas free energy $F^{id}$ is given by

$$\frac{F^{id}}{Nk_BT} = \ln\left(\frac{n2\pi\hbar^2}{mk_BT}\right) - 1 \tag{3.5}$$

or, in our units,

$$\frac{F^{id}}{Nk_BT} = 2\ln\Gamma - 1 + \ln\left(\frac{k_BT}{R_y}\right) \tag{3.6}$$

where $R_y = e^4m/2\hbar^2$ is the three-dimensional Rydberg's constant.

Equations (3.1) to (3.6) are the relations we use in our liquid phase calculations.

A. The Hypernetted Chain Method

The hypernetted chain equation has been very successful[19] in predicting the properties of the dense one component plasma in three dimensions. In this subsection we shall present the results for the two-dimensional case. The hypernetted chain integral equation for the pair correlation function is defined by the following two equations

$$g(r) - 1 = c(r) + n\int d\vec{r}\,'\,[g(r') - 1]c(|\vec{r} - \vec{r}\,'|) \tag{3.7}$$

$$\ln g(r) = g(r) - 1 - c(r) - \frac{v(r)}{k_B T} \quad , \tag{3.8}$$

where c(r) is the direct correlation function. This equation is difficult to solve for long range interactions. Following the method used recently by Springer, et al[20] we carry out a subtraction procedure to rewrite the equations in terms of short range quantities. We decompose the original potential v(r) into long and short range parts

$$v(r) = v_{lr}(r) + v_{sr}(r) = \frac{\Gamma}{r}\,\mathrm{erf}(br) + \frac{\Gamma}{r}\,[1 - \mathrm{erf}(br)] \ . \tag{3.9}$$

The parameter b is for the moment arbitrary. We denote the sum of nodal diagrams by N(r):

$$N(r) = g(r) - 1 - c(r) \quad , \tag{3.10}$$

and decompose $N(r)$ into short and long range parts

$$N_{sr}(r) = N(r) - v_{lr}(r) \tag{3.11}$$

Since at large r, $N(r) \sim \Gamma/r$, $N_{sr}(r)$ is short ranged. Similarly for the direct correlation function $c(r)$ we have

$$c_{sr}(r) = c(r) + v_{lr}(r) \quad . \tag{3.12}$$

It is now easy to see that Eqs. (3.5) and (3.6) can be solved by Fourier transforms. The set of equations to be solved are

$$N_{sr}(k) = \frac{c_{sr}(k)\,[c_{sr}(k) - \frac{2\Gamma}{r}\mathrm{Erfc}(k/2b)] - \frac{2\Gamma}{r}\mathrm{Erfc}(k/2b)}{1 - [c_{sr}(k) - \frac{2\Gamma}{r}\mathrm{Erfc}(k/2b)]} \quad , \tag{3.13}$$

$$g(r) = \exp[N_{sr}(r) - v_{sr}(r)] \quad , \tag{3.14}$$

$$c_{sr}(r) = g(r) - 1 - N_{sr}(r) \quad , \tag{3.15}$$

where

$$c_{sr}(k) = n \int e^{i\vec{k}\cdot\vec{r}} c_{sr}(r) d^2r = 4\pi \int_0^\infty J_0(kr)\, r c_{sr}(r)\, dr \quad , \tag{3.16}$$

and

$$N_{sr}(k) = n \int e^{i\vec{k}\cdot\vec{r}} N_{sr}(r) d^2r = 4\pi \int_0^\infty J_0(kr)\, r N_{sr}(r)\, dr \quad , \tag{3.17}$$

We also have for the inverse transform

$$N_{sr}(r) = \frac{1}{n(2\pi)^2} \int e^{i\vec{k}\cdot\vec{r}} N_{sr}(k) d^2k = \frac{1}{n} \int_0^\infty kN_{sr}(k) J_0(kr)\, dk \ . \qquad (3.18)$$

It is clear from Eqs. (3.7 - 3.16) that the original equation has been cast into a form which involves only short range functions, and the numerical transforms can therefore be calculated much more readily. The method is similar to the Ewald technique for calculating lattice sums, and depends on an optimum choice of the parameter b such that the functions are short ranged in both k and r space. The remaining problem is to calculate the Hankel transforms accurately. Since we will need to take transforms back and forth between r and k space, it is important that the algorithm preserves the orthogonality of Bessel functions. Such an algorithm has been worked out by Lado[21]. A significant improvement of the accuracy was obtained by calculating the zeros of the Bessel function to machine accuracy. Machine memory limitations essentially restricted us to a maximum of 200 points in r and k space. Our results are presented at the end of this section.

B. Monte Carlo Method

Our MC simulations were performed in the time-honored manner pioneered by Metropolis et al[22]. Each run had a given number of particles N, a given area A, and a fixed value of $\Gamma$. The area A was chosen to be a rectangle capable of accomodating a section of triangular close-packed lattice with periodic boundary conditions. To minimize surface effects the rectangle was chosen to be nearly square with the ratio of the x and y edges as

$$\frac{L_x}{L_y} = \frac{\sqrt{3}}{2} \qquad (3.19)$$

This shape enabled us to make runs with $4n^2$ ($n = 1, 2, 3, \ldots$) particles.

Due to the long range nature of the potential, the interaction of each particle with the other $(N - 1)$ particles in the basic rectangle, with all images of the $N$ particles, and with the uniform neutralizing background must all be included. This complete interaction can be written as

$$v(\vec{r}) = \sum_{\lambda'} \frac{\Gamma}{|\vec{r} + L_x\vec{\lambda}'|} - \frac{\Gamma}{L_x L_y} \int \frac{d^2\rho}{|\vec{r} + \vec{\rho}|} \tag{3.20}$$

where $\lambda'$ is the set of vectors generated by the basis vectors $(1,0)$ and $(0, \sqrt{3}/2)$ and where $\vec{r}$ is the distance vector between the two particles. This interparticle potential may be efficiently handled via the Ewald technique[23]. The computation proceeds in a similar way to the 3D case[12]. The result is

$$v(\vec{r}) = \frac{\Gamma}{L_x}\Big[ \sum_{\lambda'} \frac{\operatorname{erfc}(\sqrt{\alpha}\,|\vec{r}/L_x + \vec{\lambda}'|)}{|\vec{r}/L_x + \vec{\lambda}'|} - \left(\frac{\pi}{3\alpha}\right)^{\frac{1}{2}} + \frac{2}{\sqrt{3}} \sum_{\lambda''}{}' \frac{1}{|\vec{\lambda}''|} \operatorname{erfc}\left(\frac{\pi|\vec{\lambda}''|}{\sqrt{\alpha}}\right)$$
$$\times \exp\left(-2\pi i \frac{\vec{\lambda}''\cdot\vec{r}}{L_x}\right)\Big], \tag{3.21}$$

where the second sum is over a reciprocal lattice with basis $(1,0)$ and $(0,2/\sqrt{3})$. The prime on that sum denotes the exclusion of the term with $\vec{\lambda}'' = (0,0)$. The parameter $\alpha$ may be varied to achieve a balance in the rates of convergence of the two sums.

Even with the application of the Ewald technique equation (3.21) is unacceptably slow for MC calculations. To make the calculation more efficient $v(\vec{r})$ is split into two parts. The first part consists of the spherically symmetric $(\vec{\lambda}' = 0)$ term which is tabulated with a 35,000 point mesh. The remaining part of $v(\vec{r})$, which is invariant under reflections $(x \to -x,\ y \to -y)$ and inversions $(\vec{r} \to -\vec{r})$, is tabulated on a 151 x 171 point grid. With linear interpolation applied to each part of $v(\vec{r})$ the potential energy of a configuration may be efficiently calculated with an error of approximately 0.001% , which we found to be negligible.

If we now include the interaction of each particle with its own images we obtain the total interaction energy of a configuration of the N particles and images as



$$\frac{V}{k_B T} = \sum_{i<j} \frac{v(\vec{r}_{ij})}{k_B T} + \frac{V'}{k_B T} \tag{3.22}$$

The constant term is just half the Madelung energy of a rectangular lattice with sides $L_x$ and $L_y$. In our units

$$\frac{V'}{Nk_B T} = -1.09653\, \Gamma \left(\frac{\pi}{L_x L_y}\right)^{\frac{1}{2}} . \tag{3.23}$$

In our MC calculation the center of mass is not fixed. To correct for this effect the difference between the MC value for the excess internal energy $U^{MC}/NkT$ and the static energy $U_o/NkT$ of a perfect triangular close-packed lattice must be multiplied by $N/(N-1)$[24]. If we follow Hansen[12] and call the difference between the excess internal energy and the static energy the thermal contribution ($U^{th}$) to the excess internal energy

$$\frac{U^{th}}{Nk_B T} = \left(\frac{U^{MC}}{Nk_B T} - \frac{U_o}{Nk_B T}\right) \frac{N}{N-1} \qquad . \tag{3.24}$$

Our excess internal energy is then

$$\frac{U^{ex}}{Nk_B T} = \frac{U^{th}}{Nk_B T} + \frac{U_o}{Nk_B T} \qquad . \tag{3.25}$$

Here the static lattice energy is given by half the Madelung energy of the triangular close-packed lattice.

$$\frac{U_o}{Nk_BT} = -1.106103\,\Gamma \quad . \tag{3.13}$$

The liquid phase Monte Carlo runs were made with 16, 36, 64, and 100 particles. These numbers of particles, while small for three-dimensional work, are reasonable for two dimensions. The starting configurations for the runs were either a triangular close-packed lattice or a quasi-random configuration. For each run approximately 13,000 moves per particle were made and on the average 50% of these moves were accepted. Of these approximately 3,000 moves per particle were discarded in order to allow the system to lose its memory of its original configuration and reach an "equilibrium state." Since the amount of configuration space to be sampled is considerably reduced in two dimensions over three dimensions these runs represent very long Markov chains when judged by standards normally applied in three dimensions. Runs of this length are needed to accurately determine the thermal portion of the excess internal energy which is only about 1% of the total excess internal energy. From block averaging we estimate that our calculated <u>excess thermal</u> energies have errors of the order of 1%.

For the small $\Gamma$ region effects due to the small numbers of particles are not really significant; even the 16 particle runs show little effect due to the small size. For the largest values of $\Gamma$ number dependence becomes much more important. However, as can be seen from Fig. 1 the number dependence, in the energy, is essentially eliminated by the time 100 particles is reached.

The most convenient way of dealing with the HNC and MC results is with a simple and accurate fitting function.

The small $\Gamma$ expansion of Totsuji[18], mentioned in section II, gives us the low $\Gamma$ behavior of the excess internal energy. However, this expansion is not accurate for $\Gamma$ above 0.3. We have fitted our MC and HNC data up to a value of $\Gamma$ of 0.5 by the simple expedient of adding a term $c\Gamma^6$ to equation (2.9). The value of c, and all other fitting parameters, is given in table I. We have a second fitting formula for values of $\Gamma$ in the range 0.45 to 130. It is based on Hansen's[12] three-dimensional work and the fact that

$$\lim_{\Gamma\to\infty} \frac{U^{ex}}{Nk_BT} = \frac{U_o}{Nk_BT} = -1.106\,\Gamma \tag{3.27}$$

The formula is

$$\frac{U^{ex}}{Nk_BT} = \Gamma^2\left[\frac{a_1}{a_2+\Gamma} + \frac{a_3}{(a_4+\Gamma)^2} + \frac{a_5}{(a_6+\Gamma)^3} + \frac{a_7}{(a_8+\Gamma)^4}\right] \tag{3.28}$$

where the value of $a_1$ is fixed by equation (3.26). This formula accurately reproduces both our MC and HNC results with the parameters given in table I. Our MC results are presented in table II and figure 1.

We have calculated the excess free energy of the liquid phase by using equation (3.4) with equations (2.9) and (3.28). We switch between equation (2.9) and equation (3.28) at $\Gamma_o = 0.45$. Our free energy is then given by

$$\frac{F^{ex}}{Nk_BT} = \Gamma^2\left[\ln\Gamma + \gamma - 1 + \ln 2\right]$$

$$+ \Gamma^4\left[-2(\ln\Gamma)^2 + (3-2\gamma)\ln\Gamma + (1-2\gamma)(\ln 2-\tfrac{1}{2}) - \tfrac{1}{4}\right] \tag{3.29}$$

$$+ \frac{c\Gamma^6}{3}$$

for $0 \leq \Gamma \leq \Gamma_o$ and by

$$\frac{F^{ex}}{Nk_BT} = \frac{F_o^{ex}}{Nk_BT} + a_1\left[\Gamma-\Gamma_o+a_2 \ln\left(\frac{a_2+\Gamma_o}{a_2+\Gamma}\right)\right]$$

$$+ a_3\left[\ln\left(\frac{a_4+\Gamma}{a_4+\Gamma_o}\right) - \frac{\Gamma}{a_4+\Gamma} + \frac{\Gamma_o}{a_4+\Gamma_o}\right]$$

$$+ a_5\left[\frac{a_6}{2}\left(\frac{1}{(a_6+\Gamma)^2} - \frac{1}{(a_6+\Gamma_o)^2}\right) - \left(\frac{1}{1+a_6\Gamma} - \frac{1}{1+a_6\Gamma_o}\right)\right]$$

$$+ a_7\left[\frac{a_8}{3}\left(\frac{1}{(a_8+\Gamma)^3} - \frac{1}{(a_8+\Gamma_o)^3}\right) - \tfrac{1}{2}\left(\frac{1}{(a_8+\Gamma)^2} - \frac{1}{(a_8+\Gamma_o)^2}\right)\right] \tag{3.30}$$

for $\Gamma_o \leq \Gamma \leq 130$, where $F_o^{ex}/Nk_BT$ is given by equation (3.29) evaluated for $\Gamma = \Gamma_o$. Our results for the free energy are tabulated in table 2 and displayed graphically in figure 2. We agree well with the results of Totsuji[10] for the free energy. It should be noted that our Monte Carlo runs are approximately ten times longer than his. For this reason we believe our data is more accurate.

The excess specific heat at constant area may be calculated by differentiating the excess internal energy

$$\frac{C_A^{ex}}{Nk_B} = -\Gamma^2 \frac{\partial}{\partial\Gamma}\left[\frac{1}{\Gamma}\frac{U^{ex}}{Nk_BT}\right] \tag{3.31}$$

In the region $0 \leq \Gamma \leq 0.45$ we obtain

$$\frac{C_A^{ex}}{Nk_B} = -\Gamma^2\left[2\gamma + 1 + \ln 4 + 2\ln\right]$$

$$+ \Gamma^4[(2\gamma-1)4(2+3\ln 2) + 8(6\gamma-1)\ln\Gamma + 24(\ln\Gamma)^2]-5c\Gamma^6 \tag{3.32}$$

and for $0.45 \leq \Gamma \leq 130$ we get

$$\frac{C_A^{ex}}{Nk_B} = \Gamma^3\left[\frac{a_1}{a_2 + \Gamma} + \frac{2a_3}{(a_4 + \Gamma)^2} + \frac{3a_5}{(a_6 + \Gamma)^3} + \frac{4a_7}{(a_8 + \Gamma)^4}\right] - \Gamma^2\left[\frac{a_1}{a_2 + \Gamma} + \frac{a_3}{(a_4 + \Gamma)^2} + \frac{a_5}{(a_6 + \Gamma)^3} + \frac{a_7}{(a_8 + \Gamma)^4}\right] \qquad (3.33)$$

The equation of state follows from the virial theorem, equation (3.3).

Table 2 contains our results for the specific heat. Figure 3 shows our results for $C_A$ using the fitting formula and from direct Monte Carlo calculations. The latter calculation is difficult due to the large fluctuations in the data and our results are preliminary in nature. We will discuss them in more detail in section V.

## IV. SOLID PHASE CALCULATIONS

A combination of lattice dynamics and MC methods was used to compute the properties of the solid phase. The lattice dynamics calculation was performed in the manner of Bonsall and Maradudin[14]. The technique of special points[25,26] was used to efficiently calculate various thermodynamic functions by averaging functions of the frequencies over the first Brillouin zone. The lattice dynamics calculations provided us with approximations for the free energy and other thermodynamic functions and the root mean square deviation of particles from their equilibrium lattice sites. The MC calculations provided us with internal energies, and the one and two particle distribution functions for the crystalline phase. From these results we calculated the free energy and specific heat. These MC calculations were performed in the same way as in the liquid phase with the exception that all runs were started from a perfect lattice. Again runs were performed for 16, 36, 64, and 100 particles. For $\Gamma \leq 120$ we found that the deviations of the particles from their original lattice sites did not reach a steady value during runs. This value of $\Gamma$ was taken as a preliminary indication of the location of the phase transition to the liquid phase. Solid phase MC runs were made for values of $\Gamma$ between 130 and 300.

A center of mass correction was applied just as in the liquid phase. The dependence of the thermodynamic quantities on the number of particles in the simulation was found to be less severe than in the high $\Gamma$ liquid phase with the 100 particle system again well representing the infinite particle system. The prediction of harmonic lattice dynamics for the excess internal energy is

$$\frac{U^{Harm}}{Nk_BT} = 1 + \frac{U_o}{Nk_BT} \qquad (4.1)$$

The pressure is, of course, still given by equation (3.3 ).

In the harmonic approximation the total free energy is given by[27]

$$\frac{F^{Harm}}{Nk_BT} = \frac{U_o}{Nk_BT} + \frac{1}{N} \sum_{\vec{q},j} \ln\left[\sinh\left(\frac{\hbar\omega_j(\vec{q})}{2k_BT}\right)\right] \qquad (4.2)$$

where the sum is over frequencies in the first zone and $j$ is summed over the two branches. In the classical limit we get

$$\frac{F^{Harm}}{Nk_BT} = \frac{U_o}{Nk_BT} + \frac{1}{N} \sum_{\vec{q},j} \ln\left(\frac{\omega_j(\vec{q})}{\omega_o}\right) + 2\ln\left(\frac{\hbar\omega_o}{k_BT}\right) \qquad (4.3)$$

where $\omega_o^2 = \frac{e^2}{ma^3}$ . In our units we obtain:

$$\frac{F^{Harm}}{Nk_BT} = \frac{U_o}{Nk_BT} + \frac{1}{N}\sum_{qj} \ln \frac{\omega_j(q)}{\omega_o} + 3\ln\Gamma - \ln 2 + \ln\left(\frac{k_BT}{R_y}\right) \tag{4.4}$$

The values of the sums over frequencies is given for various grids in the first Brillouin zone in Table 3.

The harmonic approximation for the excess specific heat is

$$\frac{C_A^{Harm}}{Nk_B} = 1 \tag{4.5}$$

We can also calculate in the harmonic approximation root-mean-square deviation of particles from their lattice sites, $\gamma^H$.[27] It is given by

$$(\gamma^H)^2 = \langle r^2/d^2\rangle = \frac{\hbar}{m}\frac{1}{2N}\sum_{qj} \frac{1}{\omega_j(q)} \coth\left(\frac{\hbar\omega_j(q)}{2k_BT}\right) \tag{4.6}$$

where d is the near neighbor distance. In the classical limit this becomes

$$(\gamma^H)^2 = \langle r^2/d^2\rangle = \frac{1}{\Gamma}\frac{\sqrt{3}}{2\pi}\frac{1}{N}\sum_{qj}\left(\frac{\omega_o}{\omega_j(q)}\right)^2 \tag{4.7}$$

This result is tabulated for varying numbers of points in the Brillouin zone in Table 5.

An important point to note is that the small q behavior of $\omega_j(q)$ is[14]

$$\begin{aligned} \omega_1(q) &\propto \sqrt{q} \\ \omega_2(q) &\propto q \end{aligned} \tag{4.8}$$

Thus, the harmonic approximation predicts a logarithmic divergence, as the thermodynamic limit is approached, of $\gamma^H$ due to the small q behavior of

$\omega_2(q)$. This divergence has been seen[28] in molecular dynamics studies of crystalline systems of hard disks ranging in size from 100 to approximately 7,000. We have no reason to believe that it will not occur in our system. This means that Lindemann's ratio is not independent of the size of the system in two dimensions. We give a more detailed discussion of these matters in Section VI .

Our solid phase MC results are tabulated in Table 4, together with some of the lattice dynamics predictions. Our MC results are well parameterized by adding a small anharmonic correction to the harmonic excess internal energy (4.1)

$$\frac{U^{ex}}{Nk_BT} = \frac{U^{Harm}}{Nk_BT} + a\Gamma^{-1} + b\Gamma^{-2} \tag{4.9}$$

The anharmonic contribution is the first part of an expansion in powers of T or inverse powers of $\Gamma$. The values of a and b which we find are 5.0 and 560. The internal energy is displayed in Figure 1.

Given our simple result for the excess internal energy the other thermodynamic functions follow directly. We assume that in the infinite $\Gamma$ limit the harmonic free energy becomes the exact free energy. Hence, we may obtain the free energy for finite $\Gamma$ by integrating the anharmonic correction to obtain

$$\frac{F^{tot}}{Nk_BT} = \frac{F^{harm}}{Nk_BT} + \int_{\infty}^{\Gamma} (a\Gamma'^{-1} + b\Gamma'^{-2}) \frac{d\Gamma'}{\Gamma'} = \frac{F^{harm}}{NbT} - a\Gamma^{-1} - \tfrac{1}{2}b\Gamma^{-2} \tag{4.10}$$

The free energy is plotted in figure 2. By differentiating the excess internal energy according to Eq. (3.31) we obtain the excess specific heat of the solid phase,

$$\frac{C_A^{ex}}{Nk_B} = 1 + 2a\Gamma^{-1} + 3b\Gamma^{-2} . \tag{4.11}$$

Figure 3 shows this function and also our result for $C_A$ from direct Monte Carlo computation.

## V. THE PHASE TRANSITION

Using the free energies calculated in the preceeding sections we searched for a phase transition between the liquid and solid phases. Looking at table 2 we see that for the 100 particle system the liquid free energy is lower than the solid free energy for $\Gamma$ below about 130. However, this crossover point is extremely sensitive to the free energies. An error of only 0.04% in the total free energy or 0.7% in the excess thermal free energy would shift the melting point $\Gamma$ by 15. Doing a double tangent construction to determine the width of the two phase region shows that the melting and freezing points are only separated by about 0.1 in $\Gamma$.

Since the free energies lie so close it is worthwhile to seek confirmation of the location of the phase transition by looking at the behavior of systems which were started from a perfect crystal and allowed to melt. The 100 particle system started at $\Gamma = 130$ achieved an equilibrium value of the root mean square deviation of .158. This system was allowed to age for 13,000 moves per particle. The $\Gamma = 120$ particle system melted after about 2000 moves per particle. In our $N = 64$ particle runs the same behavior was observed with the $\Gamma = 130$ system attaining an equilibrium root mean square deviation of 0.153. Hence, the phase transition probably lies below a value of $\Gamma$ of 130 and above a $\Gamma$ of 120. Since metastability appears to be much less of a problem with softer potentials in two and three dimensions and the free energies are difficult and expensive to compute for such potentials,monitoring the stability of the crystal lattice is a sensible alternative for soft-potentials. The quantity $\Gamma$ is essentially a measure of the ratio of the potential and kinetic energies of the plasma. We therefore see that the system crystallizes when the potential energy is approximately one hundred times larger than the kinetic energy. This, to us, somewhat surprising result is very similar to that found in three dimensions.

Hockney and Brown[11] found a second order phase transition at $\Gamma = 95 \pm 2$ in a molecular dynamics simulation involving 10,000 particles. We have made several careful runs in the neighborhood of $\Gamma = 95$ but have found no signs of any anomaly in either the free energy or the internal energy. In figure 3 and table 2 we have presented the results of a direct calculation of the specific heat at constant area based on the fluctuations in internal energy:

$$\frac{C_A^{ex}}{Nk_B} = \frac{\Gamma^2}{N}\left[ \left\langle \left( \sum_{i<j} V(\vec{r}_{ij}) \right)^2 \right\rangle - \left\langle \sum_{i<j} V(\vec{r}_{ij}) \right\rangle^2 \right] \qquad (5.1)$$

Calculation of the specific heat in this fashion is inevitably noisy but our results are clearly incompatible with the results of Hockney and Brown[11]. They performed their calculation by starting at a low temperature, or high value of $\Gamma$, with a crystal with several grain boundaries and then increasing the temperature in steps. We interpret the discrepancy with our results as showing that they did not give their system time to achieve equilibrium at the various temperatures. It is hard to blame the discrepancy in the difference in numbers of particles; we do not see how a system which melts at a value of $\Gamma$ of 120 for 100 particles could remain stable at a $\Gamma$ of 100 for 10,000 particles. As the next section will show, traditional indicators of crystalline order, such as the mean square deviation of particles from their lattice sites, increase with the number of particles for fixed $\Gamma$. We know of no quantity which indicates increased order as the number of particles increases, in two-dimensional systems.

The order of the phase transition is an important question. A recent discussion by Kosterlitz and Thouless[29] argues that melting in two dimensions for short range forces is caused by the appearance of free dislocations as a result of the breakup of pairs (or higher combinations) of dislocations with opposing Burger's vector. Their calculation results in an analytic specific heat at the transition but the approximations they make are of the type which could easily mask a weak singularity. A recent calculation by Nelson[30], yields an essential singularity in the specific heat. Another calculation by Holz and Medeires[31] argues for a first order phase transition with short range forces and gives a rationalization for the second order phase transition observed by Hockney and Brown[11].

Young[32] has performed a calculation, similar to that of Nelson[30], paying particular attention to the angular forces between dislocation pairs, and finds qualitatively similar results. Most recently Halperin and Nelson[33] have argued that two-dimensional melting occurs in two steps. They propose that at a low temperature the breakup of dislocation pairs leads to a transition to a "liquid crystal" phase and at higher temperature the dissociation of disclination pairs yields an isotropic fluid.

We thus find the theoretical situation to be less than completely clear, especially for long range forces. Our results are compatible with a first order phase transition but our total free energy curves cross with a difference in slope of 0.03%. It may be argued that fitting the equation of state data biases one toward a first order phase transition and we are unwilling to state an order for our phase transition. All we can say is that in the thermodynamic quantities we have calculated we see no indication of any divergences.

It is our conviction that the way to proceed at this point is to attempt to use molecular dynamics to investigate the mechanism of melting and we are starting further work along these lines.

## VI. LINDEMANN'S RATIO AND SIZE DEPENDENCE

In table 4 we show values of the root mean square displacement of electrons from their original lattice sites. All of these values are for 64 or 100 particle systems with periodic boundary conditions. Examination of these quantities shows that melting occurs for a root mean square displacement of .16 $\pm$ .01 in terms of the near neighbor distance. This quantity is known as Lindemann's ratio. However, as we will see, this statement is an over simplification of the situation in two dimensional crystals.

Over 40 years ago Peierls[34] and Landau[35] argued that there would be no true long range two-dimensional crystalline order. Peierls produced an argument based on the harmonic approximation and Landau used his theory of second order phase transitions. Ten years ago these arguments were made rigorous by Mermin[15] who proved that, for every $\vec{k} \neq 0$, the Fourier component $\rho_K$ of the density must vanish in the thermodynamic limit. More precisely he showed that

$$\rho_{\vec{k}} \leq (\ln(N))^{-\frac{1}{2}} \quad . \tag{6.1}$$

$$\text{where } \rho_{\vec{k}} = \frac{1}{N} < \sum_{i=1}^{N} e^{-i\vec{k}\cdot\vec{x}_i} > . \tag{6.2}$$

He also showed that

$$<|\vec{u}(\vec{R})|^2>^{\frac{1}{2}} \;..\; \text{const}(\ln N)^{\frac{1}{2}} \tag{6.3}$$

where $\vec{u}(\vec{R})$ is the deviation of the particle from the lattice point at $\vec{R}$.

This proof is valid for potentials $\emptyset(r)$ for which

$$\emptyset(\vec{r}) - \lambda \vec{r}^{2} |\nabla^2 \emptyset(\vec{r})| \tag{6.4}$$

is integrable at $\vec{r} = \infty$ and positive and nonintegrable at $\vec{r} = 0$, both for $\lambda = 0$ and some positive finite value of $\lambda$. The 1/r potential does not meet the first criterion. Hence, the question as to whether the two-dimensional one component plasma can display long range crystalline order has not been rigorously answered at present. We do, however, find the Landau-Peierls[34,35] argument very convincing.

To investigate this question we have performed a series of Monte Carlo calculations at a value of $\Gamma$ equal to 200 and with the number of particles varying from 16 to 1024. The root mean square deviation is plotted against $(\ell n(N))^{\frac{1}{2}}$ in figure 4. For comparison the result of a lattice dynamics calculation is shown on the same graph. Due to the extremely lengthy calculations required to achieve convergence of this quantity we were not able to obtain more than a lower bound for the cases of N = 512 and N = 1024. It is seen that the points from N = 16 to N = 256 are compatible with the $\ell n(N)$ behavior but do not definitely rule out the approach of the root mean square deviation a constant value. We plan more work on this question in the near future.

In figures 5 and 6 we have displayed plots of the distribution of particles about their lattice sites for N values of 144 and 1024. The increase in the mean square deviation can be clearly seen. The one particle distribution functions are displayed in figure 8.

In his paper Mermin [15] pointed out that two-dimensional crystals, while not possessing true long range translational order, may have long range orientational order. If $\vec{R} = n_1\vec{a}_1 + n_2\vec{a}_2$ and $\vec{r}(\vec{R}) = \vec{R} + \vec{u}(\vec{R})$ then in the harmonic approximation

$$\Delta^2 = \langle[\vec{r}(\vec{R}+\vec{a}_1) - \vec{r}(\vec{R})]\cdot[\vec{r}(\vec{R}+\vec{a}_1) - \vec{r}(\vec{R})]\rangle \rightarrow |\vec{a}_1|^2 \text{ as } |\vec{R}-\vec{R}'| \rightarrow \infty \qquad (6.5)$$

In figure 7 we show the results for $\Delta^2$ at $\Gamma = 200$ for various numbers of particles. It is seen that this quantity rapidly approaches a constant value independent of N.

We believe that we have established that the lattice displacements in the one component plasma behave in a very similar way to those of the hard disk system [28]. There is a loss of translational long range order as the size of the system increases. On the other hand there appears to be long range orientational order. The full implications of this observation must await a more detailed investigation of larger systems.

## VII. ONE AND TWO PARTICLE DISTRIBUTION FUNCTIONS

In figure 8 we have plotted the distribution function, n(r), for particles about their lattice sites. The single particle distribution function is defined so that $n(r)d\vec{r}$ is the probability of finding a particular particle within a volume element $d\vec{r}$ at a point removed from the lattice site by a displacement $\vec{r}$. The logarithm of n(r) has been plotted as a function of the distance from the lattice site squared. Hence, if the distribution of particles about their lattice sites were Gaussian, the points would fall on a straight line. The normalization has been arbitrarily chosen so that n(r) = 1 for the point with the smallest value of r.

Two effects are illustrated in this plot. For the two plots with N = 64 we can see the effect of lowering $\Gamma$ from 300 to 200. In addition, the effect of changing N from 64 to 1024 for $\Gamma = 200$ is evident. In none of the cases is n(r) truly Gaussian. The result for $\Gamma = 300$ is approximately Gaussian but the results for $\Gamma = 200$, although more spread out than n(r) for $\Gamma = 300$, appear to be cutoff more steeply than a Gaussian distribution. Our results contrast with the results of Young and Alder[28] who find that densely packed hard disks form a Gaussian distribution but that at lower density the distribution decays more slowly than a Gaussian distribution. Thus, the considerable differences between hard disks and 1/r particles seem to produce opposite deviations from Gaussian behavior as the melting transition is approached.

The radial distribution function g(r) is defined by the equation,

$$g(r) = \frac{N(N-1)}{\rho^2} \frac{1}{Q_N} \int \ldots \int \exp[-\sum_{i<j} v(r_{ij})]d\vec{r}_3 \ldots d\vec{r}_N \tag{7.1}$$

We have calculated values for g(r) function for $\Gamma = 36$, $\Gamma = 90$, and $\Gamma = 120$. These are tabulated in table 6 and plotted in figures 9, 10, and 11. For $\Gamma = 90$ the HNC result for g(r) is plotted for comparison with the Monte Carlo result. The perhaps surprising feature is that g(r) shows considerably more structure than the corresponding values of g(r) given by Hansen[12] for the three-dimensional case. This, however, may be a general feature of two-dimensional simple fluids as both Fehder[36] and Tsien and Valleau[37] found the height of the first peak in g(r) to fall between 3 and 4 for two-dimensional Lennard-Jones fluids. The HNC result for g(r) shown for $\Gamma = 90$ also shows correspondingly more structure than three-dimensional HNC results.

Finally, we have also calculated the structure factor S(k) which is defined via

$$S(k) = \frac{1}{N} < \rho_{\vec{k}} \rho_{-\vec{k}} > \tag{7.2}$$

where

$$\rho_k = \sum_{i=1}^{N} e^{i\vec{k}\cdot\vec{r}_i} \tag{7.3}$$

The $\vec{k}$ vectors used are those corresponding with the reciprocal lattice generated via the periodic boundary conditions associated with the N-particle basic Monte Carlo rectangle. To determine S(k) we directly used the definition (7.2) with (7.3). In Table 7 and figures 12 and 13 our results for S(k) are illustrated for $\Gamma = 36$ and $\Gamma = 90$. For $\Gamma = 90$ we also present the result of our HNC calculation. Just as in the case of g(r) these show more structure than the three-dimensional results of Hansen[12]. We found it difficult to get a good estimate of the height of S(k) at the first peak but it is clear that it will be larger than the value of 2.85 found at freezing in many three-dimensional systems[38].

The Debye-Hückel result for S(k)[6]

$$S(k) = \frac{k}{k + 2\Gamma} \tag{7.4}$$

provides the correct low k behavior for S(k). However, for our smallest values of k the Monte Carlo values of S(k) have already risen above the Debye-Hückel

## VIII. CONCLUSIONS

In this paper we have presented the results of a Monte Carlo calculation of the properties of particles interacting via the 1/r potential in two dimensions. In particular, we have emphasized the nature of the ordered phase and attempted to show how the dimensionality has influenced the nature of the order. The second main point is the phase transition itself. Much work is currently underway in two-dimensional melting and much remains to be done. We hope that experimentalists will soon observe an ordered phase of two-dimensional electrons. This should be possible with lower temperature experiments as higher values of $\Gamma$ can be achieved at lower densities. In addition, as figure 14 shows, quantum effects, as measured by the ratio of $r_s$ and the de Broglie thermal wavelength, will become less important in the neighborhood of the phase transition if it is observed at lower temperatures.

One of us (SC) would like to thank Chia-Wei Woo and the Materials Research Center of Northwestern University for their help during the early days of this work.

This work was supported primarily by the National Science Foundation through the Cornell Materials Science Center Grant No. DMR-76-81083, technical report #3074 and by the National Aeronautics and Space Administration Grant No. NGR-33-010-188.

*Present address: Department of Physics, Hartwick College, Oneonta, New York 13820.

+Present address: Department of Physics, University of California at San Diego, La Jolla, California 92093.

## REFERENCES


1. R.S. Crandall and R. Williams, Phys. Lett. A 34, 404 (1971).
2. E.P. Wigner, Trans. Faraday Soc. 34, 678 (1938).
3. A.V. Chaplik, Sov. Phys. - JETP 35, 395 (1971).
4. R.S. Crandall, Phys. Rev. A 8, 2136 (1973).
5. P.M. Platzman and H. Fukuyama, Phys. Rev. B 10, 3150 (1974).
6. A.L. Fetter, Phys. Rev. B 10, 3739 (1974).
7. M.W. Cole, Rev. Mod. Phys. 46, 451 (1974).
8. T.R. Brown and C.C. Grimes, Phys. Rev. Lett. 29, 1233 (1972).
9. Y.P. Monarkha and V.B. Shikin, Sov. Phys. - JETP 41, 710 (1976).
10. H. Totsuji, Phys. Rev. A17, 399 (1978).
11. R.W. Hockney and T.R. Brown, J. Phys. C 8, 1813 (1975).
12. J.P. Hansen, Phys. Rev. A 8, 3096 (1973).
13. E.L. Pollock and J.P. Hansen, Phys. Rev. A 8, 3110 (1973).
14. L. Bonsall and A.A. Maradudin, Phys. Rev. B 15, 1959 (1977).
15. N.D. Mermin, Phys. Rev. 171, 272 (1968).
16. P. Debye and E. Hückel, Physik, Z. 24, 185 (1923).
17. R.H. Brout and P. Carruthers, Lectures on the Many-Electron Problem (Interscience, New York, 1963).
18. H. Totsuji, J. Phys. Soc. Jpn. 39, 253 (1975); 40, 857 (1976).
19. K.C. Ng, J. Chem. Phys. 61, 2680 (1974).
20. J.F. Springer, M.A. Pokrant, and F.A. Stevens, Jr., J. Chem. Phys. 58, 4863 (1973).
21. F. Lado, J. Comp. Phys. 8, 417 (1971).
22. N. Metropolis, A.W. Rosenbluth, M.N. Rosenbluth, A.M. Teller, and E. Teller, J. Chem. Phys. 21, 1087 (1953).
23. P.P. Ewald, Ann. Phys. (Leipz.) 64, 253 (1921); see also B.R.A. Nijboer and F.W. DeWette , Physica 23, 309 (1957).

24. W.G. Hoover, M. Ross, K.W. Johnson, D. Henderson, J.A. Barker, and B.C. Brown, J. Chem. Phys. 52, 4931 (1970).

25. D.J. Chadi and M.L. Cohen, Phys. Rev. B 8, 5747 (1973).

26. S.L. Cunningham, Phys. Rev. B10, 4988 (1974).

27. A.A. Maradudin, E.W. Montroll, and G.H. Weiss, Theory of Lattice Dynamics In the Harmonic Approximation (Academic, New York, 1963).

28. D.A. Young and B.J. Alder, J. Chem. Phys. 60, 1254 (1974).

29. J.M. Kosterlitz and D.J. Thouless, J. Phys. C 6, 1181 (1973).

30. D.R. Nelson, to be published.

31. A. Holz and J.T.N. Medeiros, Phys. Rev. B17, 1161 (1978).

32. A.P. Young, to be published.

33. B.I. Halperin and D.R. Nelson, Phys. Rev. Lett. 41, 121 (1978).

34. R.E. Peierls, Helv. Phys. Acta 7, 81 (1923); Ann. Inst. Henri Poincare 5, 177 (1935).

35. L.D. Landau, Phys. Z. Sowjet 11, 26 (1937).

36. P.L. Fehder, J. Chem. Phys. 52, 791 (1970).

37. F. Tsein and J.P. Valleau, Mol. Phys. 27, 177 (1974).

38. J.P. Hansen and D. Schiff, Mol. Phys. 25, 1281 (1973).

## Figure Captions

Fig. 1 The excess thermal internal energy as a function of $\Gamma$. The points are the results of Monte Carlo calculations with the triangles representing a 16 particle system, the circles a 36 particle system, the squares a 64 particle system and the diamonds a 100 particle system.

Fig. 2 The excess thermal free energy as a function of $\Gamma$. The circles give the results of a calculation based on the hypernetted chain integral equation, the triangles show the results of the Monte Carlo liquid state calculation, the diamonds show the predictions of lattice dynamics in the harmonic approximation, and the squares show the results of our Monte Carlo solid state calculations.

Fig. 3 The excess specific heat as a function of $\Gamma$. The points give the result of direct Monte Carlo calculation based on equation (5.1). The solid line shows the result of calculating the specific heat via equations (3.33) and (4.11) which were obtained from fitting the Monte Carlo results for the internal energy.

Fig. 4 The root mean square deviations of particles from their lattice sites as a function of the square root of the logarithm of the number of particles. The root mean square deviation is measured in terms of the near neighbor distance, d. The solid circles are the results of Monte Carlo calculations for 16, 36, 64, 100, 144, 256, 576, and 1024 particles. The point for 1024 particles represents only a lower bound. The circles represent the prediction of lattice dynamics in the harmonic approximation. The squares represent the results of a molecular dynamics calculation for hard disks by Young and Alder[28]. The hard disk calculations have $V/V_o = 1.20$ where $V_o$ is the close packed volume.

Fig. 5 This figure shows the superimposed positions of the particles for 100 different Monte Carlo configurations, each separated by 4 passes. A pass is defined as one attempted move per particle. In this simulation $\Gamma = 200$ and $N = 144$. Roughly speaking, this represents a short time picture of the crystal.

Fig. 6 This figure shows the superimposed positions of the particles for 100 different Monte Carlo configurations, each separated by 4 passes. A pass is defined as one attempted move per particle. In this case $\Gamma = 200$ and $N = 1024$. If this figure is compared with figure 5, the additional effect of the long wavelength phonons for 1024 particles may be seen. To see the long wavelength oscillations in particle positions look down the rows from a vantage point almost in the plane of the paper.

Fig. 7 The angular correlation $\Delta^2$, defined in equation (6.5), as a function of the distance, R, between pairs of particles for $\Gamma = 200$. Both $\Delta^2$ and R are measured in terms of the near neighbor distance. The results are for Monte Carlo calculations with 144, 256, 576, and 1024 particles. In each case $\Delta^2$ differs only very slightly from 1, thus demonstrating the angular order observed in the crystal.

Fig. 8 The single particle distribution function as a function of r where r is measured in units of the near neighbor distance. The triangles are for 1024 particles with $\Gamma = 200$, the squares are for 64 particles with $\Gamma = 200$, and the circles are for 64 particles $\Gamma = 300$. The normalization has been chosen so that $n(r) = 1$ for the first point.

Fig. 9 The radial distribution function, $g(r)$, as a function of interparticle distance. The points were produced via Monte Carlo calculation with 100 particles and are for $\Gamma = 36$. The distance is measured in terms of the ion sphere radius, $a = 1/(\pi n)^{\frac{1}{2}}$, where $n$ is the density.

Fig. 10 The radial distribution function, $g(r)$, for $\Gamma = 90$. The triangles are the results of Monte Carlo simulation with 100 particles and the circles were calculated by solving the hypernetted chain equation. Distances are measured in terms of the ion sphere radius.

Fig. 11 The radial distribution function, $g(r)$, for $\Gamma = 120$. The points are the result of Monte Carlo simulation with 100 particles. Distance is measured in terms of the ion sphere radius.

Fig. 12 The structure factor, $S(k)$, for $\Gamma = 36$. The points resulted from Monte Carlo calculation with 100 particles. The wavenumber, $k$, is measured in terms of the inverse ion sphere radius.

Fig. 13 The structure factor, $S(k)$, for $\Gamma = 90$. The triangles are the result of Monte Carlo calculation while the circles were calculated via solution of the hypernetted chain integral equation. The wavenumber, $k$, is measured in terms of the inverse ion sphere radius.

Fig. 14 A density versus temperature plot which shows the location of the predicted phase transition. Only the region of temperature greater than about $1^{\circ}K$ and density less than approximately $2 \times 10^{9} cm^{-2}$ have been explored experimentally. The line where the de Broglie thermal wavelength is one quarter of the near neighbor distance has been included to give an indication of the region where quantum mechanical effects become important.

TABLE I

Fitting parameters for the liquid phase results:

$c = -9.290414$

| | MC | HNC |
|---|---|---|
| $a_1$ | -1.106103 | -1.102071 |
| $a_2$ | .765873 | .799066 |
| $a_3$ | .775448 | .951230 |
| $a_4$ | .261904 | .201743 |
| $a_5$ | -1.202048 | -1.593872 |
| $a_6$ | .957986 | .131187 |
| $a_7$ | - | - .232854 |
| $a_8$ | - | .536553 |

Solid phase parameters: $a = 4.986$, $b = 561.1$

TABLE II

| $N$ | $\Gamma$ | $U^{th}/Nk_BT$ | $F^{tot}/Nk_BT$ | $C_A^{ex}/Nk_B$ |
|---|---|---|---|---|
| 64 | 1 | .32 | - .61 | .16 |
| 64 | 2 | .43 | - 1.46 | .26 |
| 64 | 5 | .61 | - 4.30 | .40 |
| 64 | 10 | .75 | - 9.36 | .52 |
| 64 | 20 | .91 | - 19.84 | .66 |
| 64 | 30 | 1.01 | - 30.52 | .76 |
| 64 | 40 | 1.08 | - 41.28 | .82 |
| 64 | 50 | 1.14 | - 52.09 | .89 |
| 100 | 60 | 1.19 | - 62.93 | .94 |
| 64 | 70 | 1.23 | - 73.81 | 1.00 |
| 100 | 80 | 1.25 | - 84.70 | .87 |
| 64 | 90 | 1.29 | - 95.61 | 1.16 |
| 100 | 100 | 1.33 | -106.54 | 1.06 |
| 100 | 110 | 1.34 | -117.47 | 1.36 |
| 100 | 120 | 1.32 | -128.42 | 1.37 |

The thermodynamic functions of the liquid phase. The internal energy has had the ideal gas and static lattice contributions subtracted from it and the specific heat has had the ideal gas contribution subtracted. The number of particles, N, is the number of particles in the Monte Carlo run.

TABLE III

| $N$ | $\langle\omega_o^2/\omega^2\rangle$ | $\langle\omega_o/\omega\rangle$ | $\langle\omega/\omega_o\rangle$ | $\langle ln(\omega/\omega_o)\rangle$ |
|---|---|---|---|---|
| 4 | 6.63 | 3.13 | 1.67 | -.599 |
| 16 | 8.88 | 3.39 | 1.63 | -.677 |
| 36 | 10.38 | 3.49 | 1.63 | -.693 |
| 64 | 11.43 | 3.53 | 1.63 | -.698 |
| 100 | 12.25 | 3.56 | 1.63 | -.700 |
| 144 | 12.91 | 3.58 | 1.63 | -.702 |
| 196 | 13.47 | 3.59 | 1.63 | -.702 |

The results of our lattice dynamics calculation are presented in the following table. N represents the number of points summed over in the Brillouin zone. The angular prackets denote the average of the various functions of frequency. The characteristic frequency $\omega_o^2 = e^2/ma^3$.

TABLE IV

| $N$ | $\Gamma$ | $U^{th}/Nk_BT$ | $F^{tot}/Nk_BT$ | $C_A^{ex}/Nk_BT$ | $\langle r^2/d^2 \rangle$ |
|---|---|---|---|---|---|
| 100 | 130 | 1.06 | -139.37 | 1.25 | .16 |
| 100 | 140 | 1.06 | -150.35 | 1.15 | .15 |
| 100 | 150 | 1.03 | -161.34 | .98 | .14 |
| 100 | 170 | 1.04 | -183.33 | 1.13 | .13 |
| 100 | 190 | 1.04 | -205.34 | 1.09 | .12 |
| 64 | 220 | 1.03 | -238.37 | 1.10 | .11 |
| 64 | 250 | 1.03 | -271.42 | 1.03 | .099 |
| 64 | 300 | 1.03 | -326.54 | 1.08 | .092 |

The thermodynamic functions of the solid phase. The internal energy has had the ideal gas and static lattice contributions subtracted from it and the specific heat has had the ideal gas contribution subtracted. The number of particles, N, is the number of particles in the Monte Carlo run. The column headed $\langle r^2/d^2 \rangle$ gives the root mean square deviation of particles from their lattice sites.

TABLE V

| $N$ | $\langle r^2/d^2 \rangle_{MC}$ | $\langle r^2/d^2 \rangle_{LD}$ |
|---|---|---|
| 16 | .09 | .11 |
| 36 | .10 | .12 |
| 64 | .11 | .12 |
| 100 | .12 | .13 |
| 144 | .12 | .13 |
| 256 | .13 | .14 |
| 512 | .13 | .14 |
| 1024 | >.13 | .15 |

This table gives the root mean square deviation if particles from their lattice sites for $\Gamma = 200$ and various numbers of particles in the basic MC rectangle. The predictions of lattice dynamics in the harmonic approximation are also presented.

TABLE VI

Monte Carlo

| r | g(r; Γ=36) | g(r; Γ=90) | r | g(r; Γ=36) | g(r; Γ=90) |
|---|---|---|---|---|---|
| 1.06 | .01 | .00 | 4.31 | .89 | .71 |
| 1.11 | .02 | .00 | 4.37 | .89 | .71 |
| 1.17 | .06 | .00 | 4.43 | .89 | .71 |
| 1.23 | .13 | .00 | 4.48 | .89 | .72 |
| 1.28 | .25 | .01 | 4.54 | .91 | .76 |
| 1.34 | .44 | .05 | 4.60 | .93 | .79 |
| 1.40 | .66 | .16 | 4.66 | .95 | .84 |
| 1.46 | .94 | .37 | 4.71 | .95 | .89 |
| 1.51 | 1.22 | .73 | 4.77 | .98 | .94 |
| 1.57 | 1.46 | 1.21 | 4.83 | 1.00 | 1.00 |
| 1.63 | 1.68 | 1.72 | 4.89 | 1.02 | 1.06 |
| 1.69 | 1.81 | 2.18 | 4.94 | 1.03 | 1.11 |
| 1.74 | 1.87 | 2.49 | 5.00 | 1.05 | 1.15 |
| 1.80 | 1.86 | 2.63 | 5.06 | 1.05 | 1.18 |
| 1.86 | 1.81 | 2.55 | 5.11 | 1.06 | 1.21 |
| 1.91 | 1.71 | 2.33 | 5.17 | 1.07 | 1.22 |
| 1.97 | 1.57 | 2.06 | 5.23 | 1.06 | 1.22 |
| 2.03 | 1.44 | 1.75 | 5.28 | 1.06 | 1.22 |
| 2.09 | 1.30 | 1.45 | 5.34 | 1.06 | 1.19 |
| 2.14 | 1.17 | 1.20 | 5.40 | 1.05 | 1.17 |
| 2.20 | 1.06 | .99 | 5.46 | 1.04 | 1.14 |
| 2.26 | .95 | .81 | 5.51 | 1.03 | 1.10 |
| 2.31 | .87 | .70 | 5.57 | 1.02 | 1.06 |
| 2.37 | .79 | .60 | 5.63 | 1.01 | 1.03 |
| 2.43 | .75 | .52 | 5.69 | 1.00 | .99 |
| 2.48 | .70 | .48 | 5.74 | .99 | .95 |
| 2.54 | .67 | .45 | 5.80 | .98 | .92 |
| 2.60 | .66 | .44 | 5.86 | .98 | .89 |
| 2.66 | .66 | .44 | 5.91 | .97 | .87 |
| 2.71 | .66 | .45 | 5.97 | .97 | .85 |
| 2.77 | .69 | .47 | 6.03 | .96 | .85 |
| 2.83 | .72 | .52 | 6.09 | .96 | .85 |
| 2.89 | .76 | .56 | 6.14 | .96 | .85 |
| 2.94 | .80 | .64 | 6.20 | .97 | .87 |
| 3.00 | .87 | .71 | 6.26 | .97 | .89 |
| 3.06 | .92 | .80 | 6.31 | .97 | .91 |
| 3.11 | .99 | .91 | 6.37 | .98 | .93 |
| 3.17 | 1.04 | 1.03 | 6.43 | .98 | .95 |
| 3.23 | 1.09 | 1.14 | 6.48 | 1.00 | .98 |
| 3.28 | 1.14 | 1.25 | 6.54 | 1.00 | 1.01 |
| 3.34 | 1.17 | 1.35 | 6.60 | 1.01 | 1.03 |
| 3.40 | 1.19 | 1.44 | 6.66 | 1.01 | 1.06 |
| 3.46 | 1.21 | 1.48 | 6.71 | 1.02 | 1.07 |
| 3.51 | 1.21 | 1.49 | 6.77 | 1.03 | 1.10 |
| 3.57 | 1.19 | 1.48 | 6.83 | 1.02 | 1.10 |
| 3.63 | 1.19 | 1.45 | 6.89 | 1.02 | 1.11 |
| 3.69 | 1.17 | 1.39 | 6.94 | 1.02 | 1.10 |
| 3.74 | 1.13 | 1.31 | 7.00 | 1.02 | 1.10 |
| 3.80 | 1.10 | 1.22 | 7.06 | 1.02 | 1.09 |
| 3.86 | 1.06 | 1.14 | 7.11 | 1.01 | 1.08 |
| 3.91 | 1.03 | 1.06 | 7.17 | 1.01 | 1.06 |

# TABLE VI

(continued)



| r | g(r; Γ=36 | g(r; Γ=90) | r | g(r; Γ=36) | g(r; Γ=90) |
|---|---|---|---|---|---|
| 3.97 | 1.00 | .97 | 7.23 | 1.00 | 1.05 |
| 4.03 | .96 | .90 | 7.28 | 1.00 | 1.03 |
| 4.09 | .94 | .84 | 7.34 | 1.00 | 1.01 |
| 4.14 | .92 | .79 | 7.40 | 1.00 | .99 |
| 4.20 | .91 | .75 | 7.46 | .99 | .98 |
| 4.26 | .90 | .72 | 7.51 | 1.00 | .97 |

Monte Carlo

Hypernetted Chain

| r | g(r; Γ=36) | g(r; Γ=90) | r | g(r; Γ=120) | r | g(r; Γ=90) |
|---|---|---|---|---|---|---|
| 7.57 | .99 | .94 | 1.30 | .01 | 1.17 | .01 |
| 7.63 | .99 | .94 | 1.45 | .20 | 1.30 | .12 |
| 7.69 | .99 | .93 | 1.60 | 1.31 | 1.44 | .67 |
| 7.74 | .99 | .92 | 1.75 | 2.72 | 1.57 | 1.53 |
| 7.80 | .99 | .92 | 1.90 | 2.68 | 1.70 | 2.20 |
| 7.86 | .99 | .93 | 2.06 | 1.70 | 1.84 | 1.96 |
| 7.91 | .99 | .93 | 2.21 | .90 | 1.97 | 1.61 |
| 7.97 | .99 | .94 | 2.36 | .51 | 2.10 | 1.25 |
| 8.03 | 1.00 | .95 | 2.51 | .36 | 2.24 | .98 |
| 8.09 | .99 | .97 | 2.67 | .35 | 2.37 | .80 |
| 8.14 | .99 | .98 | 2.82 | .44 | 2.50 | .70 |
| 8.20 | 1.00 | .99 | 2.97 | .63 | 2.64 | .65 |
| | | | 3.12 | .94 | 2.77 | .66 |
| | | | 3.28 | 1.30 | 2.90 | .72 |
| | | | 3.43 | 1.56 | 3.04 | .83 |
| | | | 3.58 | 1.59 | 3.17 | .99 |
| | | | 3.73 | 1.41 | 3.31 | 1.14 |
| | | | 3.89 | 1.12 | 3.44 | 1.24 |
| | | | 4.04 | .85 | 3.57 | 1.25 |
| | | | 4.19 | .66 | 3.71 | 1.19 |
| | | | 4.34 | .59 | 3.84 | 1.10 |
| | | | 4.49 | .64 | 3.97 | 1.02 |
| | | | 4.65 | .78 | 4.11 | .95 |
| | | | 4.80 | .99 | 4.24 | .90 |
| | | | 4.95 | 1.20 | 4.37 | .88 |
| | | | 5.10 | 1.32 | 4.51 | .88 |
| | | | 5.26 | 1.31 | 4.64 | .91 |
| | | | 5.41 | 1.20 | 4.77 | .95 |
| | | | 5.56 | 1.06 | 4.91 | 1.00 |
| | | | 5.71 | .94 | 5.04 | 1.05 |
| | | | 5.87 | .83 | 5.18 | 1.07 |
| | | | 6.02 | .77 | 5.31 | 1.08 |
| | | | 6.17 | .78 | 5.44 | 1.06 |
| | | | 6.32 | .86 | 5.58 | 1.04 |
| | | | 6.48 | .98 | 5.71 | 1.01 |
| | | | 6.63 | 1.12 | 5.84 | .98 |
| | | | 6.78 | 1.19 | 5.98 | .97 |
| | | | 6.93 | 1.19 | 6.11 | .96 |
| | | | 7.09 | 1.12 | 6.24 | .96 |

TABLE VI

(continued)

| | | Hypernetted Chain | |
|---|---|---|---|
| r | g(r; Γ=120) | r | g(r; Γ=90) |
| 7.24 | 1.03 | 6.38 | .97 |
| 7.39 | .95 | 6.51 | .98 |
| 7.54 | .89 | 6.64 | 1.00 |
| 7.69 | .87 | 6.78 | 1.02 |
| 7.85 | .88 | 6.91 | 1.02 |
| 8.00 | .92 | 7.05 | 1.03 |
| 8.15 | .99 | 7.18 | 1.02 |
| | | 7.31 | 1.02 |
| | | 7.45 | 1.00 |
| | | 7.58 | .99 |
| | | 7.71 | .99 |
| | | 7.85 | .98 |
| | | 7.98 | .98 |
| | | 8.11 | .99 |
| | | 8.25 | .99 |
| | | 8.38 | 1.00 |

Monte Carlo and hypernetted chain results for the radial distribution function, g(r), for $\Gamma$ = 36, 90, and 120. Distance is given in units of the ion sphere radius.

# TABLE VII

## Monte Carlo

| k | S(k; Γ=36) | S(k; Γ=90) |
|---|---|---|
| 1.40 | .04 | .02 |
| 1.69 | .06 | .02 |
| 1.96 | .09 | .04 |
| 2.16 | .12 | .05 |
| 2.36 | .16 | .08 |
| 2.55 | .23 | .10 |
| 2.72 | .32 | .16 |
| 2.86 | .41 | .21 |
| 3.02 | .63 | .35 |
| 3.14 | .78 | .52 |
| 3.29 | 1.11 | .83 |
| 3.43 | 1.43 | 1.46 |
| 3.52 | 1.80 | 2.04 |
| 3.66 | 1.94 | 3.37 |
| 3.78 | 2.08 | 3.36 |
| 3.88 | 2.05 | 2.89 |
| 3.99 | 1.98 | 2.41 |
| 4.08 | 1.81 | 1.90 |
| 4.22 | 1.49 | 1.38 |
| 4.29 | 1.38 | 1.24 |
| 4.38 | 1.27 | .95 |
| 4.50 | 1.10 | .87 |
| 4.59 | 1.06 | .75 |
| 4.66 | .97 | .69 |
| 4.76 | .93 | .67 |
| 4.84 | .91 | .64 |
| 4.98 | .81 | .56 |
| 5.03 | .81 | .60 |
| 5.15 | .78 | .53 |
| 5.27 | .76 | .57 |
| 5.36 | .75 | .53 |
| 5.75 | .74 | .54 |
| 5.58 | .74 | .57 |
| 5.74 | .76 | .62 |
| 5.91 | .76 | .63 |
| 6.10 | .80 | .71 |
| 6.36 | .87 | .82 |
| 6.77 | .97 | 1.06 |

## Hypernetted Chain Equation

| k | S(k; Γ=90) |
|---|---|
| 0.75 | .01 |
| 0.90 | .01 |
| 1.06 | .01 |
| 1.22 | .02 |
| 1.37 | .0[illegible] |
| 1.53 | .03 |
| 1.69 | .04 |
| 1.85 | .05 |
| 2.00 | .06 |
| 2.16 | .09 |
| 2.32 | .12 |
| 2.47 | .17 |
| 2.63 | .24 |
| 2.79 | .34 |
| 2.95 | .51 |
| 3.10 | .78 |
| 3.26 | 1.18 |
| 3.42 | 1.69 |
| 3.57 | 2.14 |
| 3.73 | 2.26 |
| 3.89 | 2.07 |
| 4.04 | 1.75 |
| 4.20 | 1.45 |
| 4.36 | 1.23 |
| 4.52 | 1.06 |
| 4.67 | .94 |
| 4.83 | .85 |
| 4.99 | .79 |
| 5.14 | .75 |
| 5.30 | .73 |
| 5.46 | .71 |
| 5.62 | .71 |
| 5.77 | .72 |
| 5.93 | .73 |
| 6.09 | .76 |
| 6.24 | .80 |
| 6.40 | .84 |
| 6.56 | .90 |
| 6.72 | .96 |
| 6.87 | 1.03 |
| 7.03 | 1.10 |
| 7.19 | 1.15 |
| 7.34 | 1.19 |
| 7.50 | 1.20 |

Monte Carlo and hypernetted chain results for the structure factor, S(k), for Γ = 36, 90, and 120. Wavenumber is measured in terms of the inverse ion sphere radius.

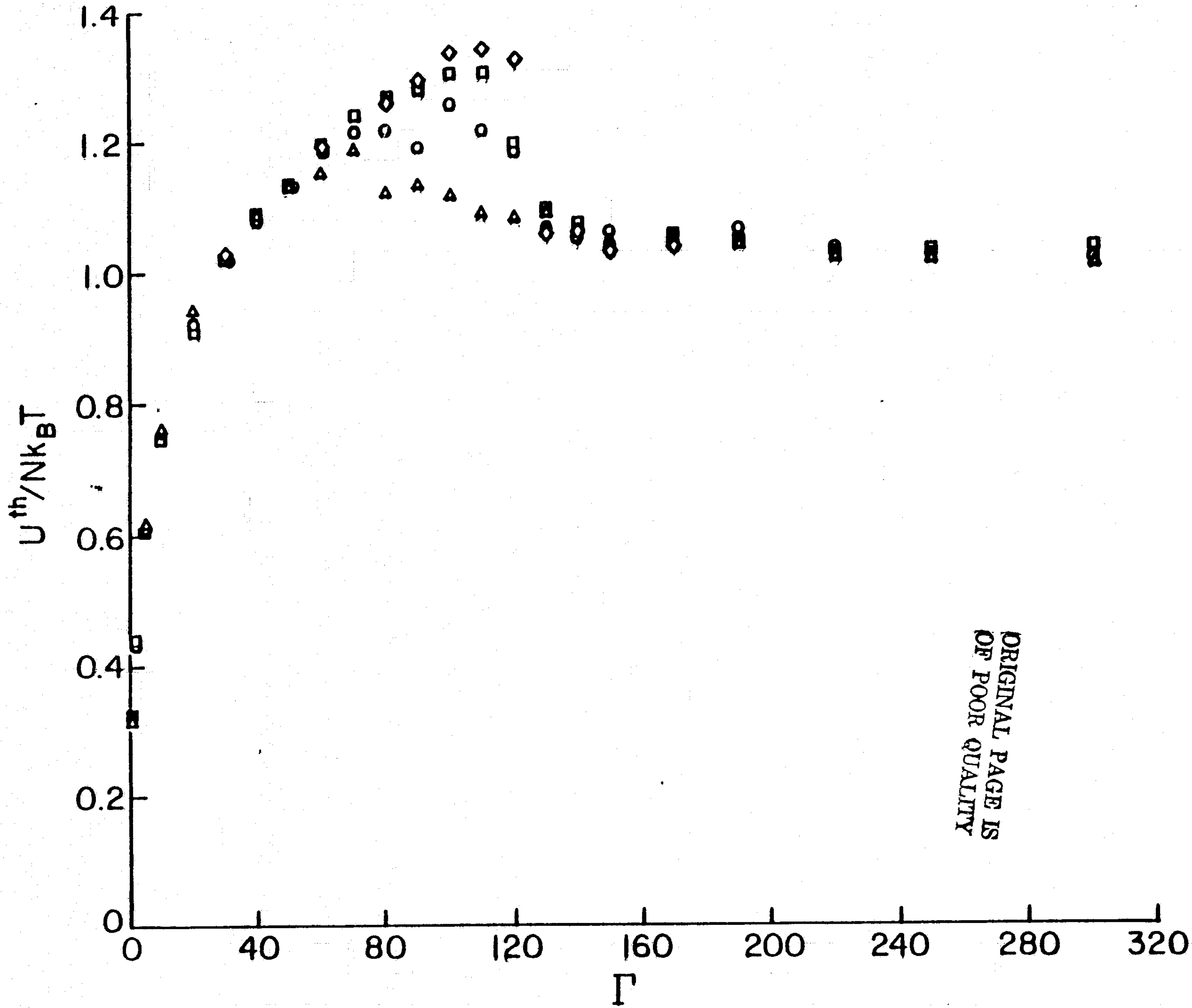
1.4
1.2
1.0
0.8
0.6
0.4
0.2
0
$U^{th}/Nk_BT$
0
40
80
120
160
200
240
280
320
Γ

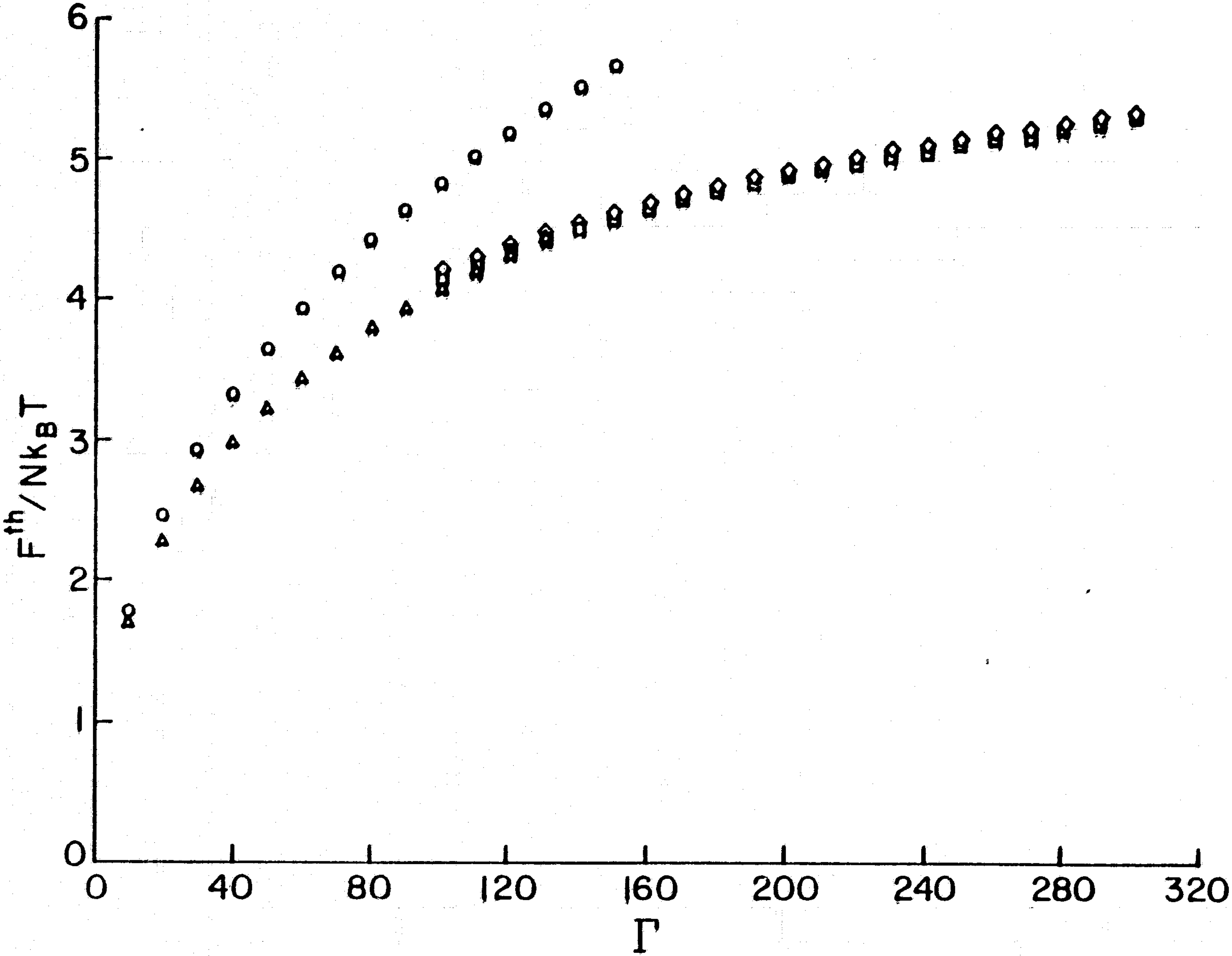

6
5
4
3
2
1
0
0
40
80
120
160
200
240
280
320
$\Gamma$
$F^{th}/Nk_BT$

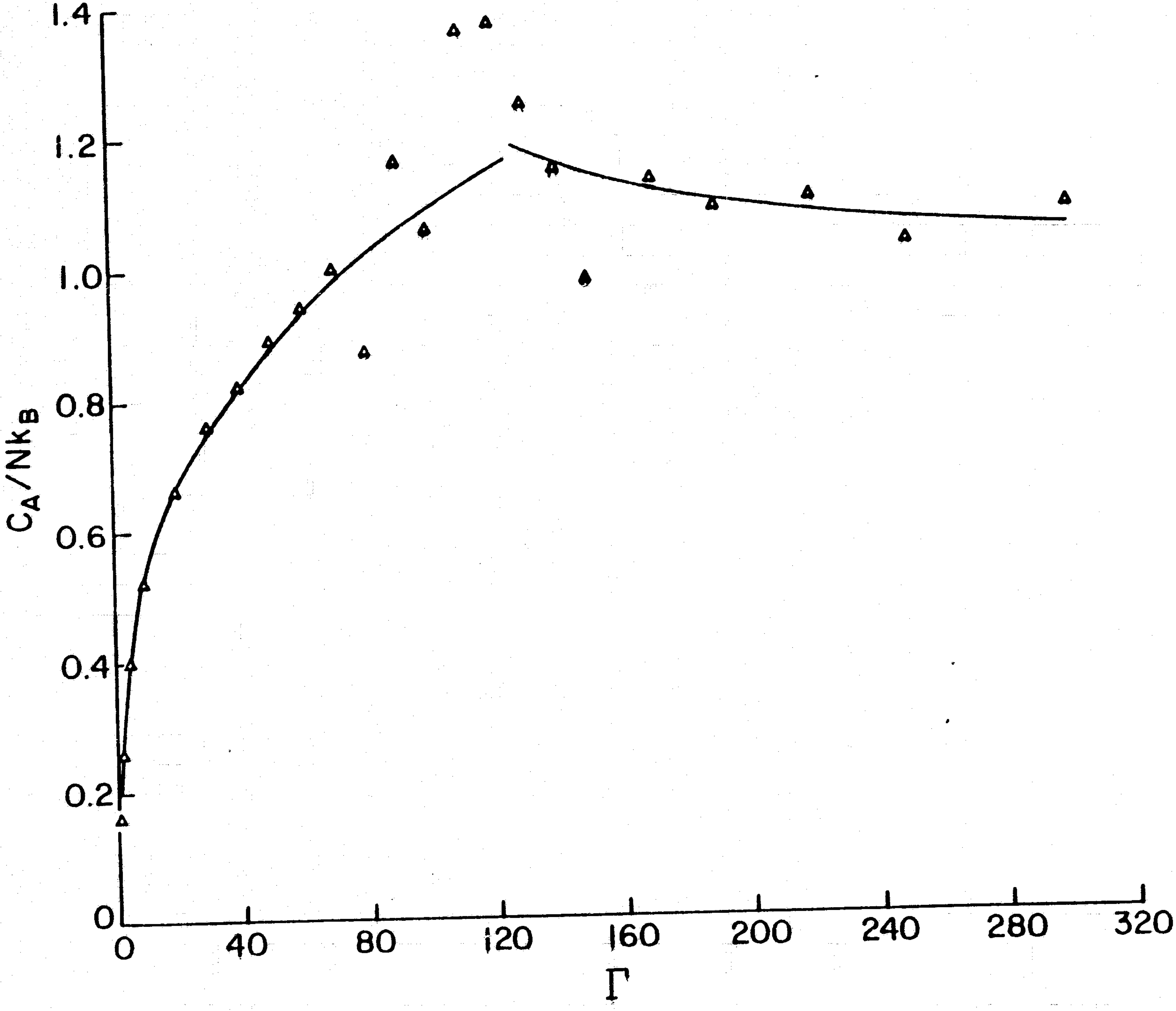

1.4
1.2
1.0
0.8
0.6
0.4
0.2
0
$C_A/Nk_B$
0
40
80
120
160
200
240
280
320
Γ

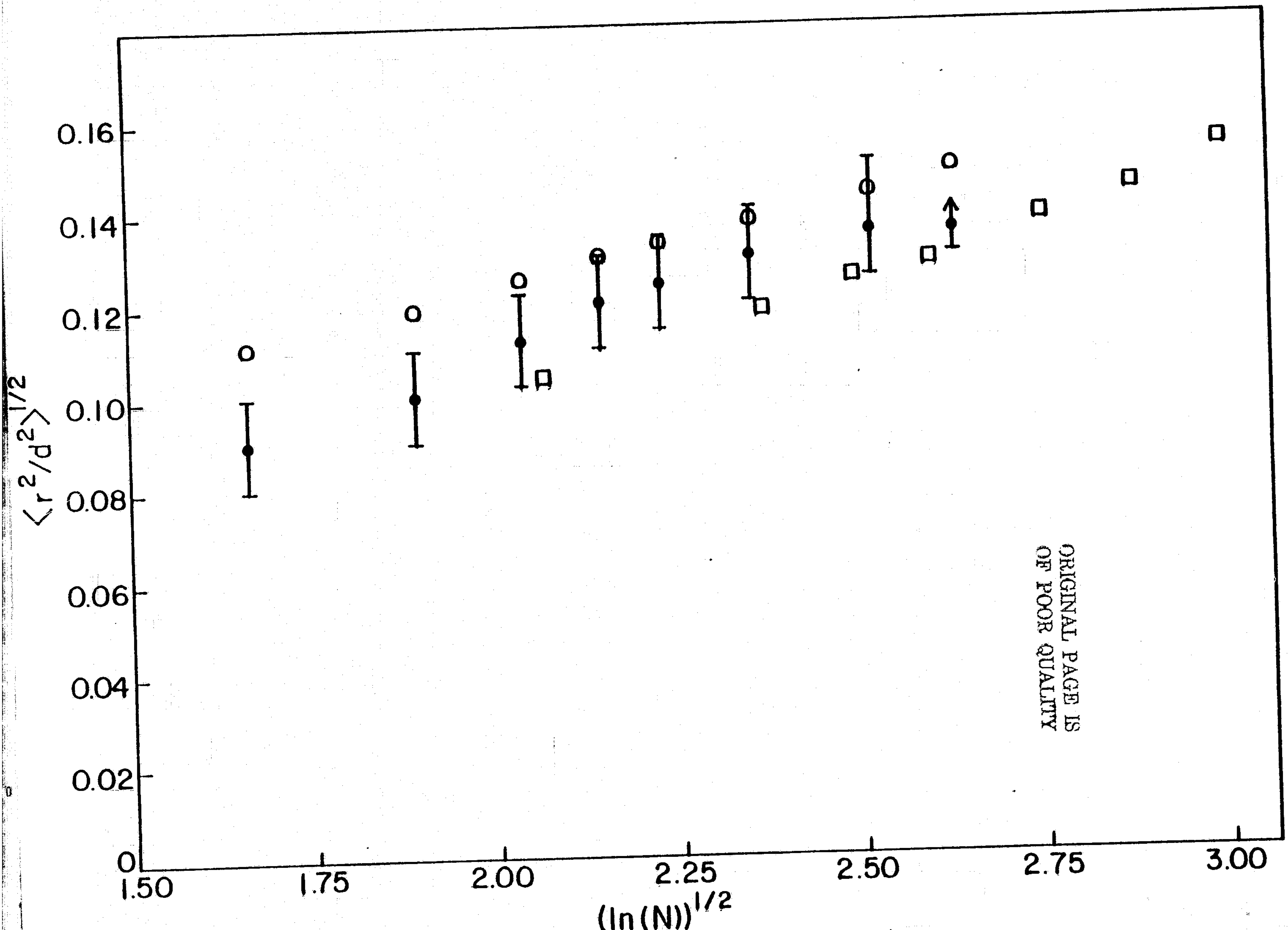
0.16
0.14
0.12
0.10
0.08
0.06
0.04
0.02
0
1.50
1.75
2.00
2.25
2.50
2.75
3.00
$\langle r^2/d^2 \rangle^{1/2}$
$(\ln(N))^{1/2}$

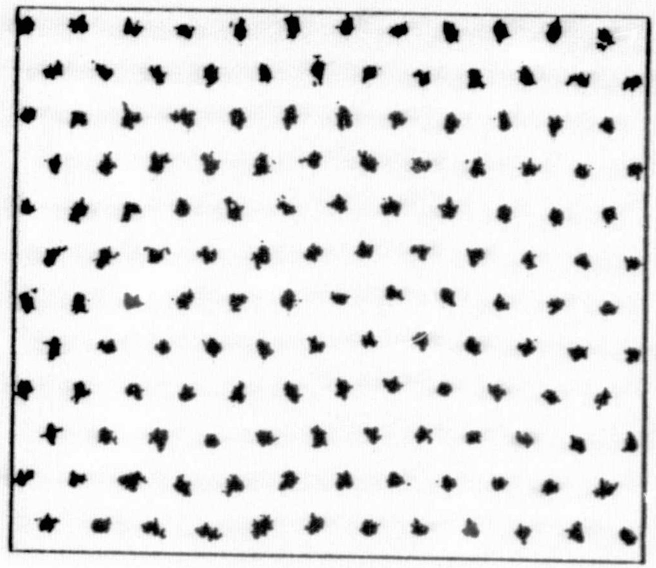

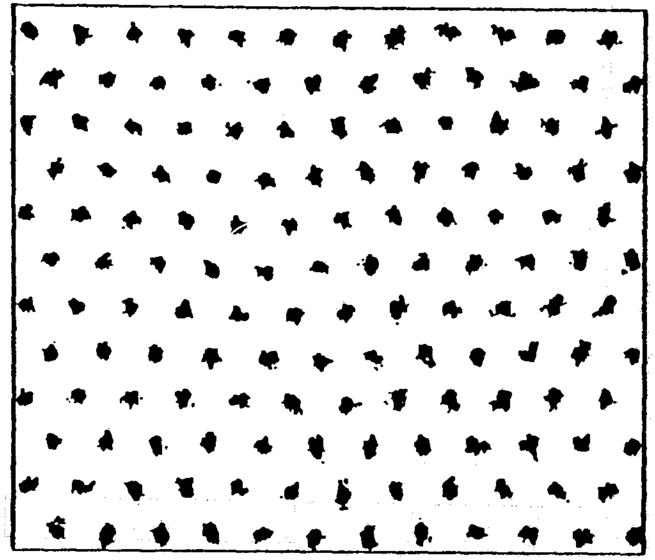

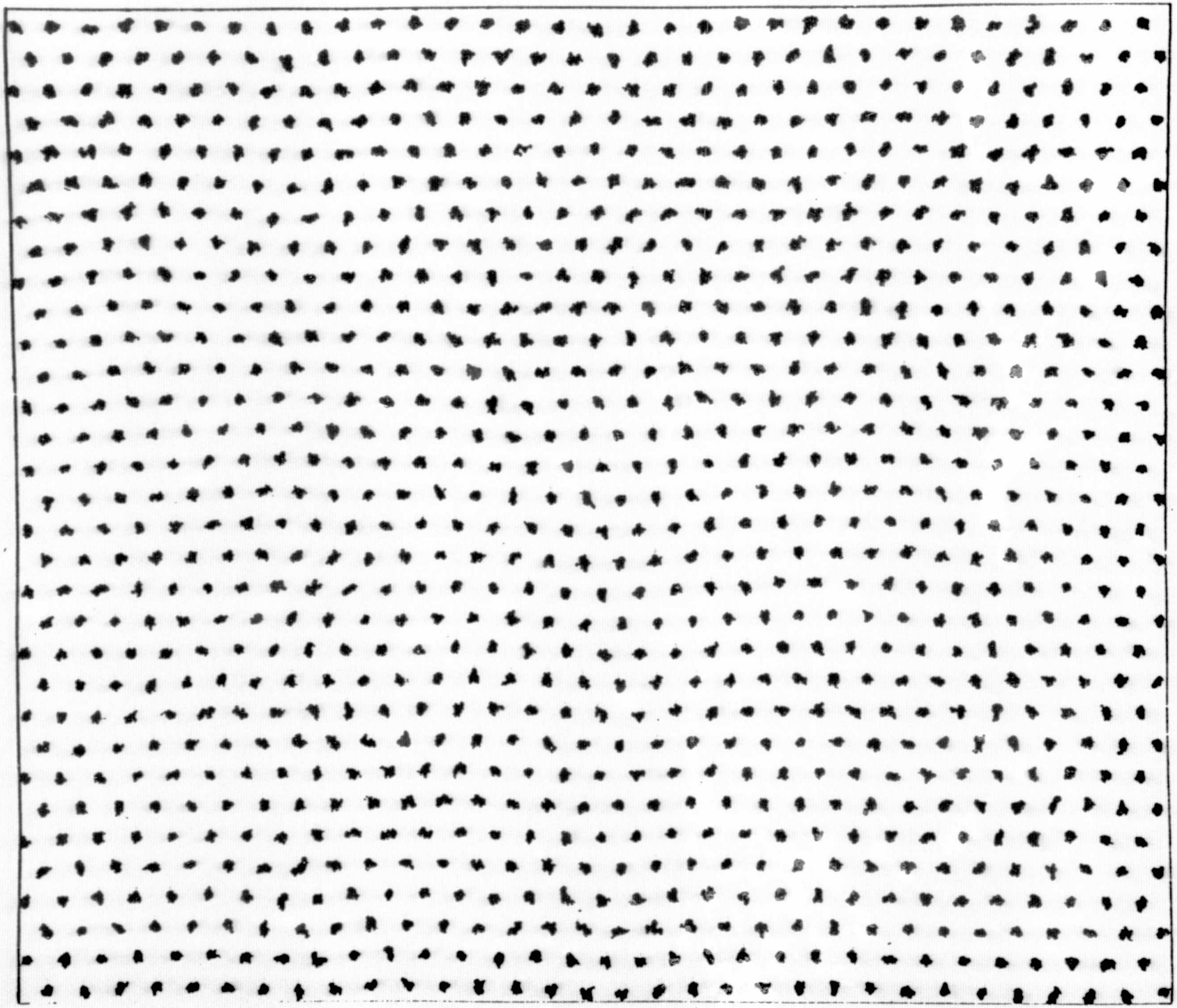

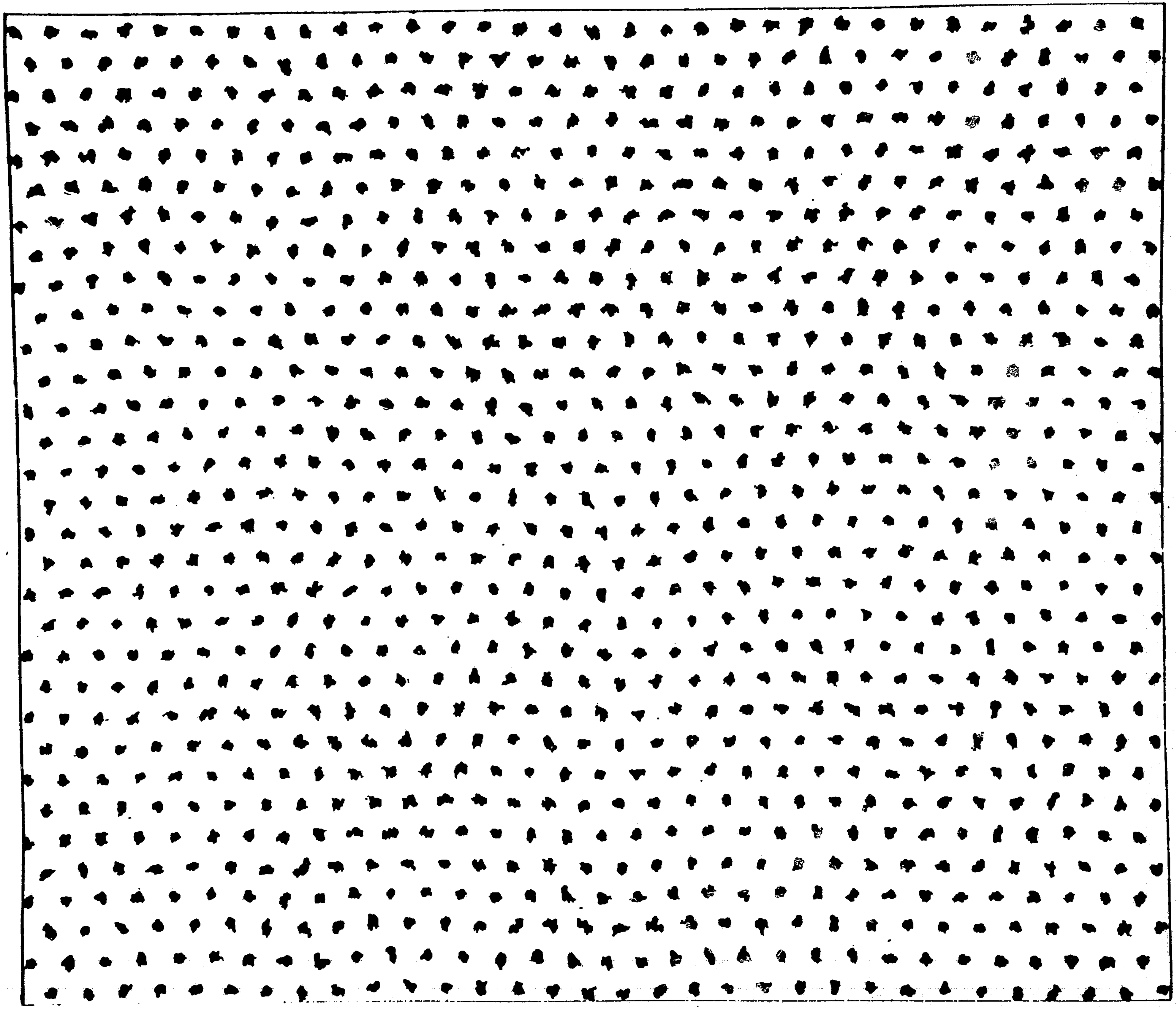

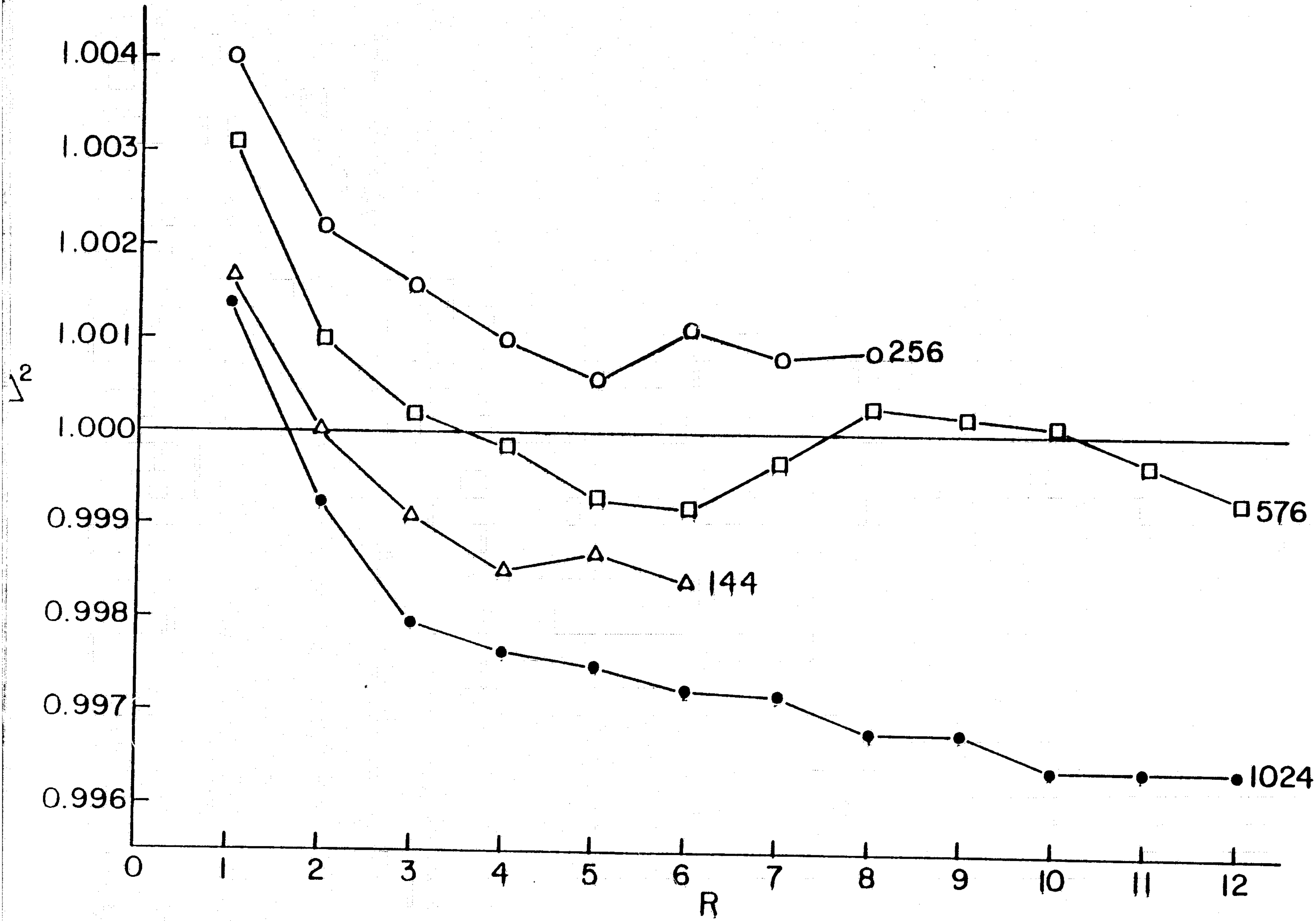

1.004
1.003
1.002
1.001
1.000
0.999
0.998
0.997
0.996
$\nu^2$
0
1
2
3
4
5
6
7
8
9
10
11
12
R
256
576
144
1024

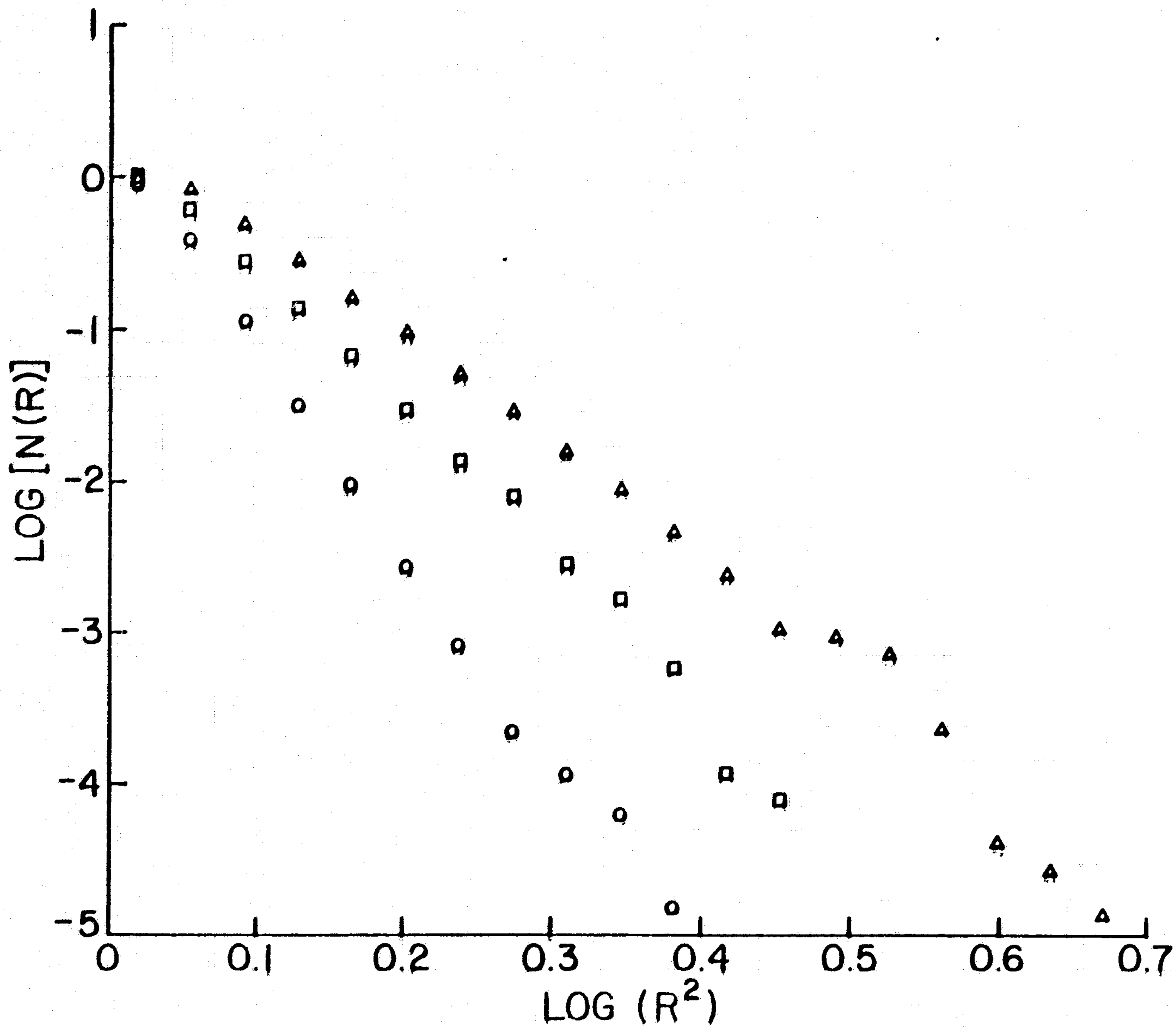

LOG [N(R)]
LOG ($R^2$)
1
0
-1
-2
-3
-4
-5
0
0.1
0.2
0.3
0.4
0.5
0.6
0.7

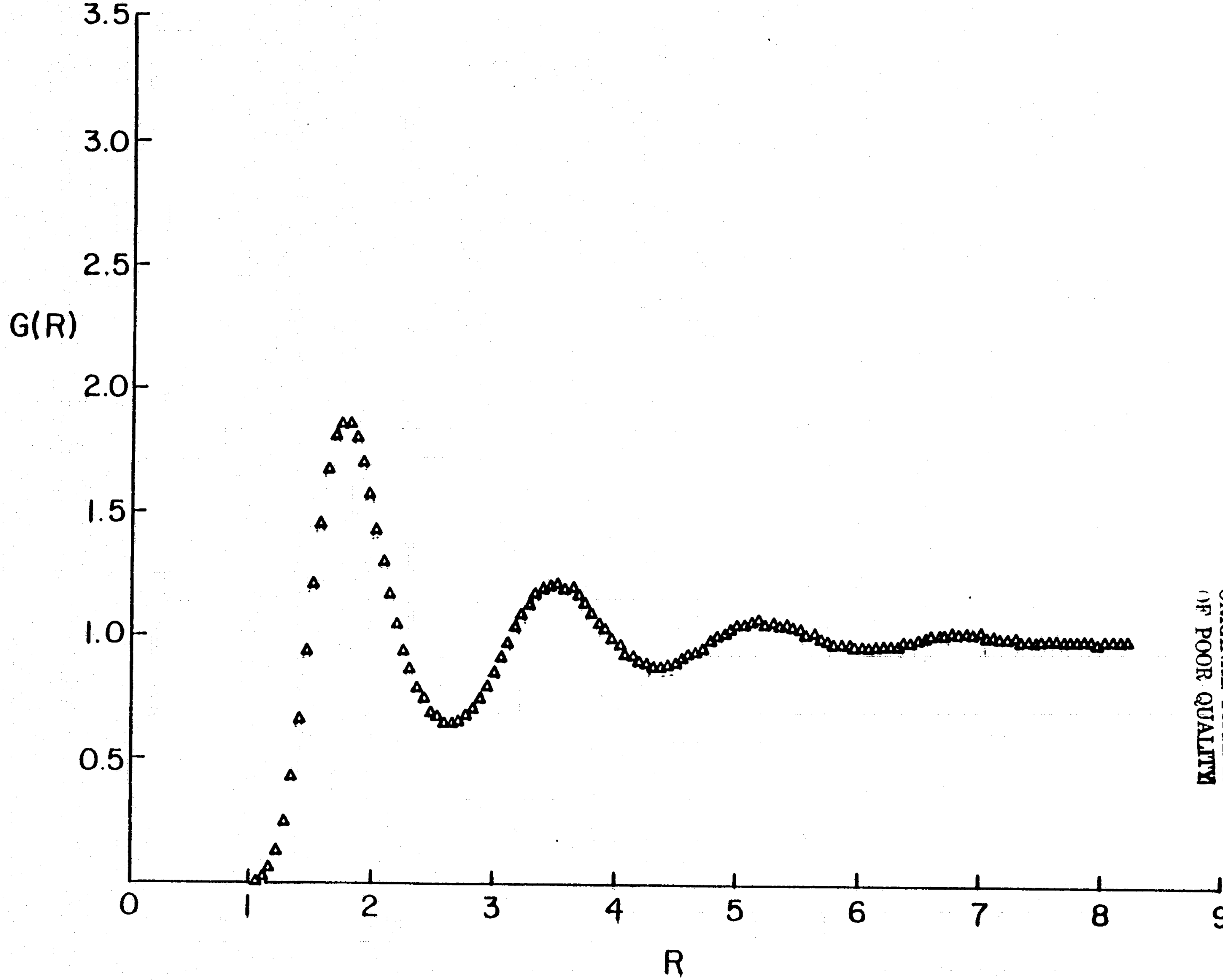


ORIGINAL PAGE IS
OF POOR QUALITY

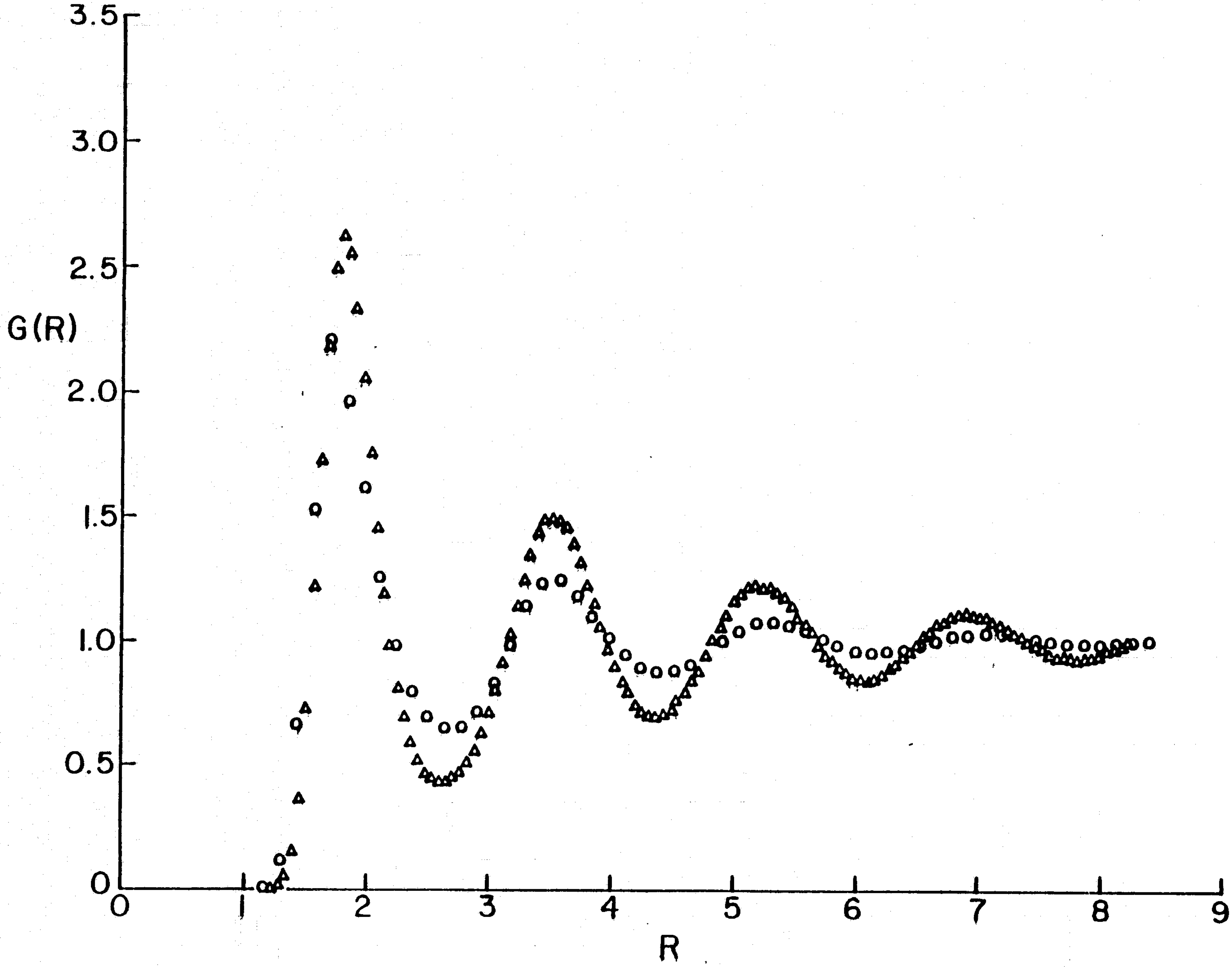

3.5
3.0
2.5
G(R)
2.0
1.5
1.0
0.5
0
0
1
2
3
4
5
6
7
8
9
R

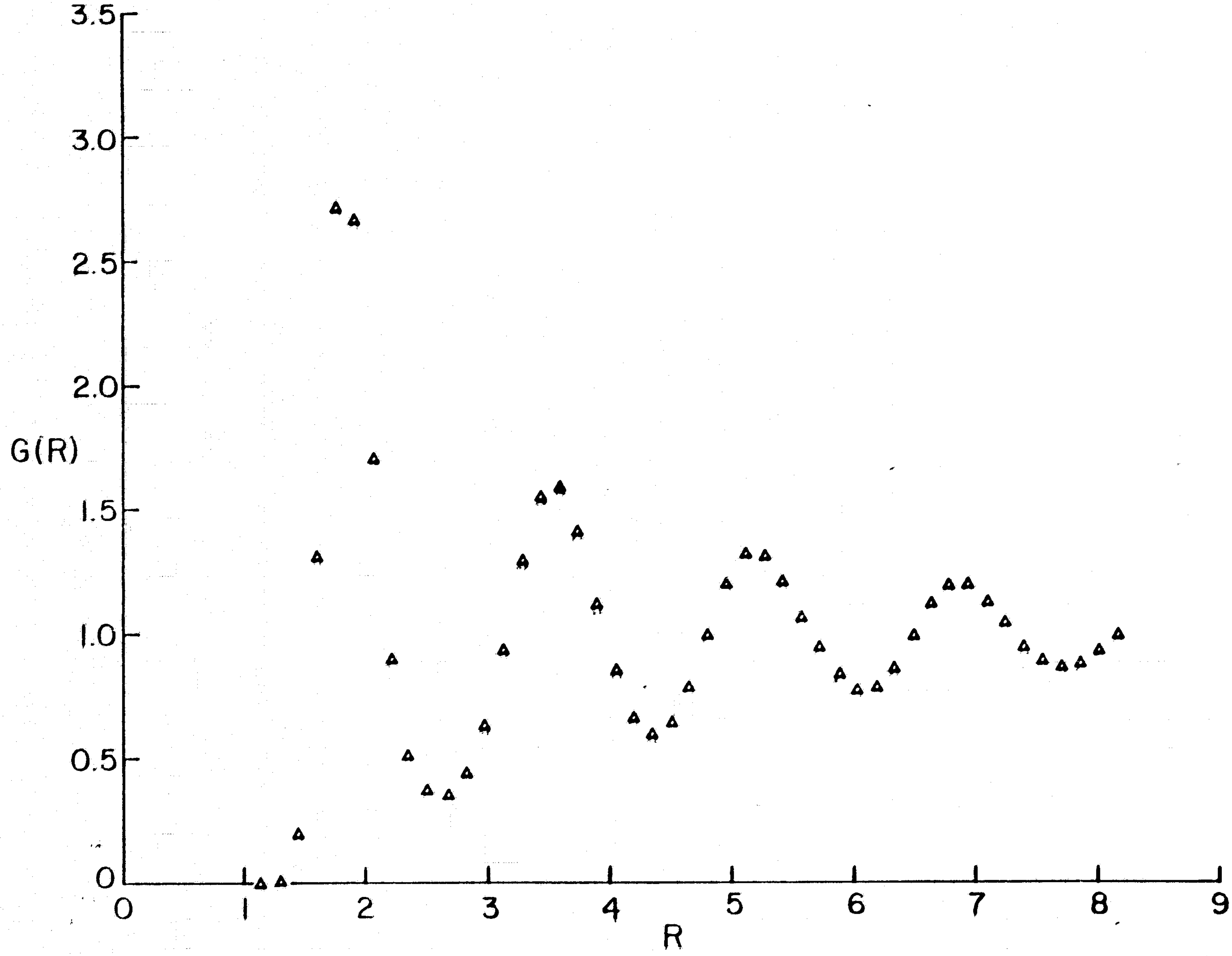
3.5
3.0
2.5
2.0
1.5
1.0
0.5
0
G(R)
0
1
2
3
4
5
6
7
8
9
R

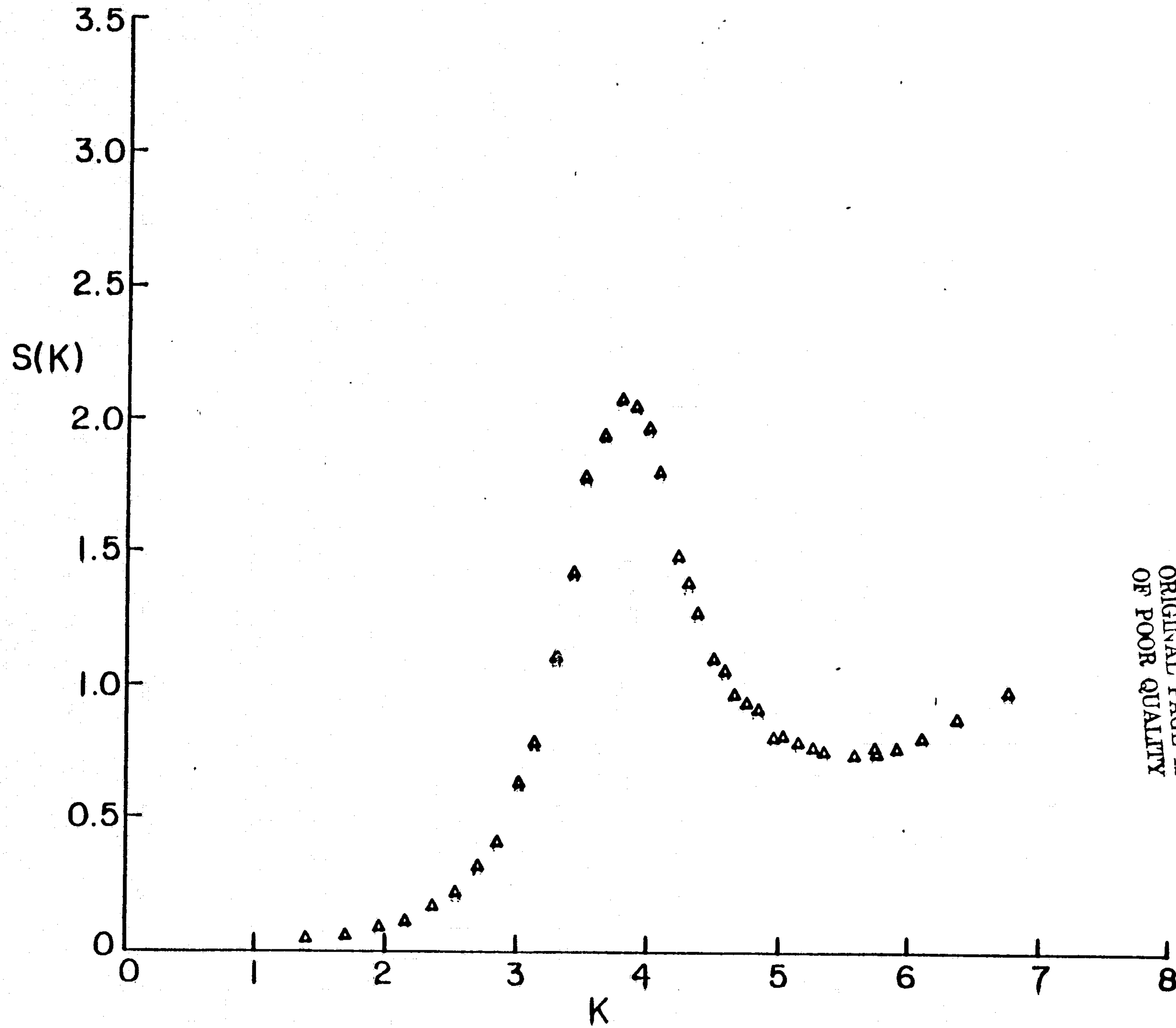

S(K)
K
0
0.5
1.0
1.5
2.0
2.5
3.0
3.5
1
2
3
4
5
6
7
8

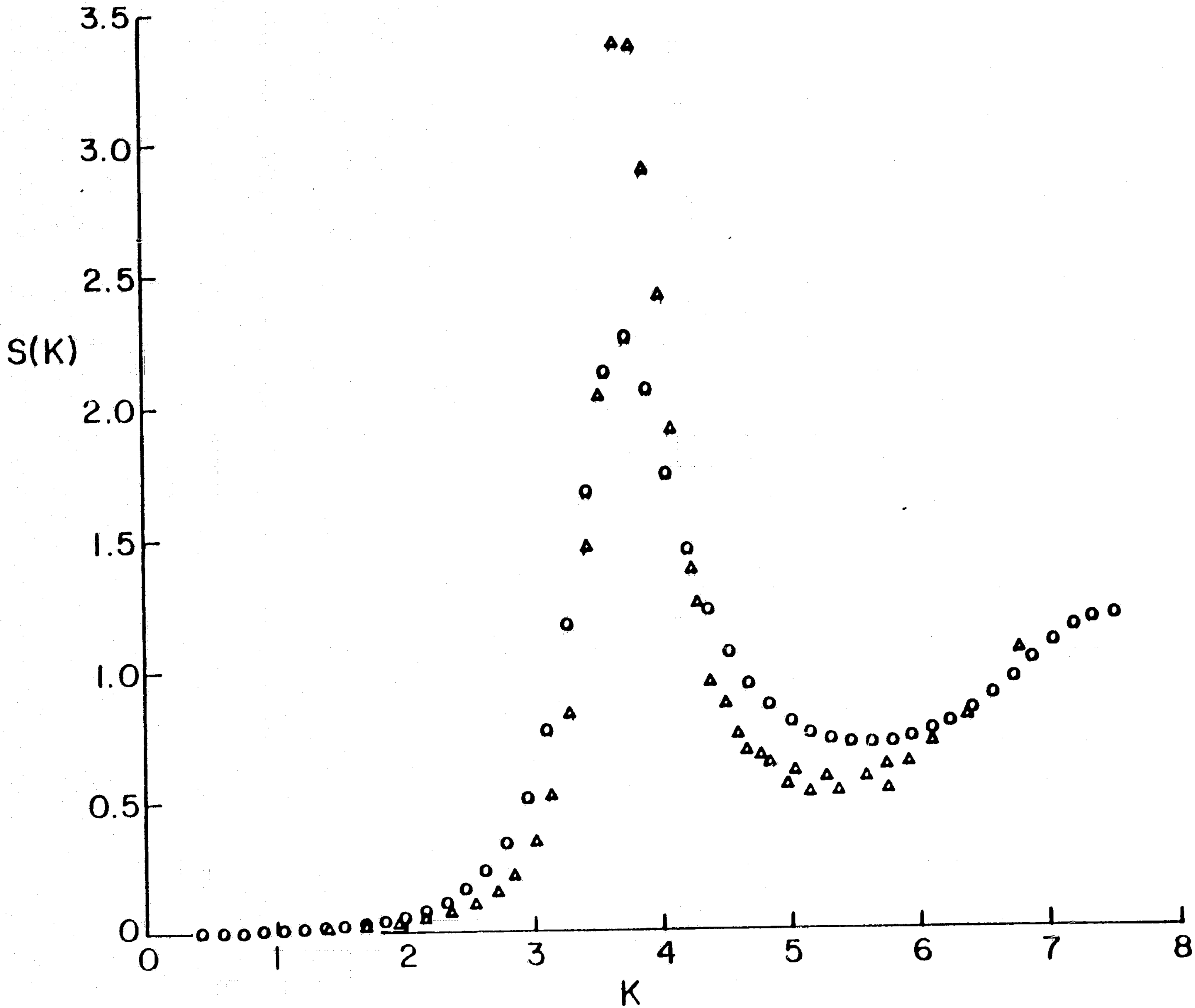

S(K)
3.5
3.0
2.5
2.0
1.5
1.0
0.5
0
0
1
2
3
4
5
6
7
8
K

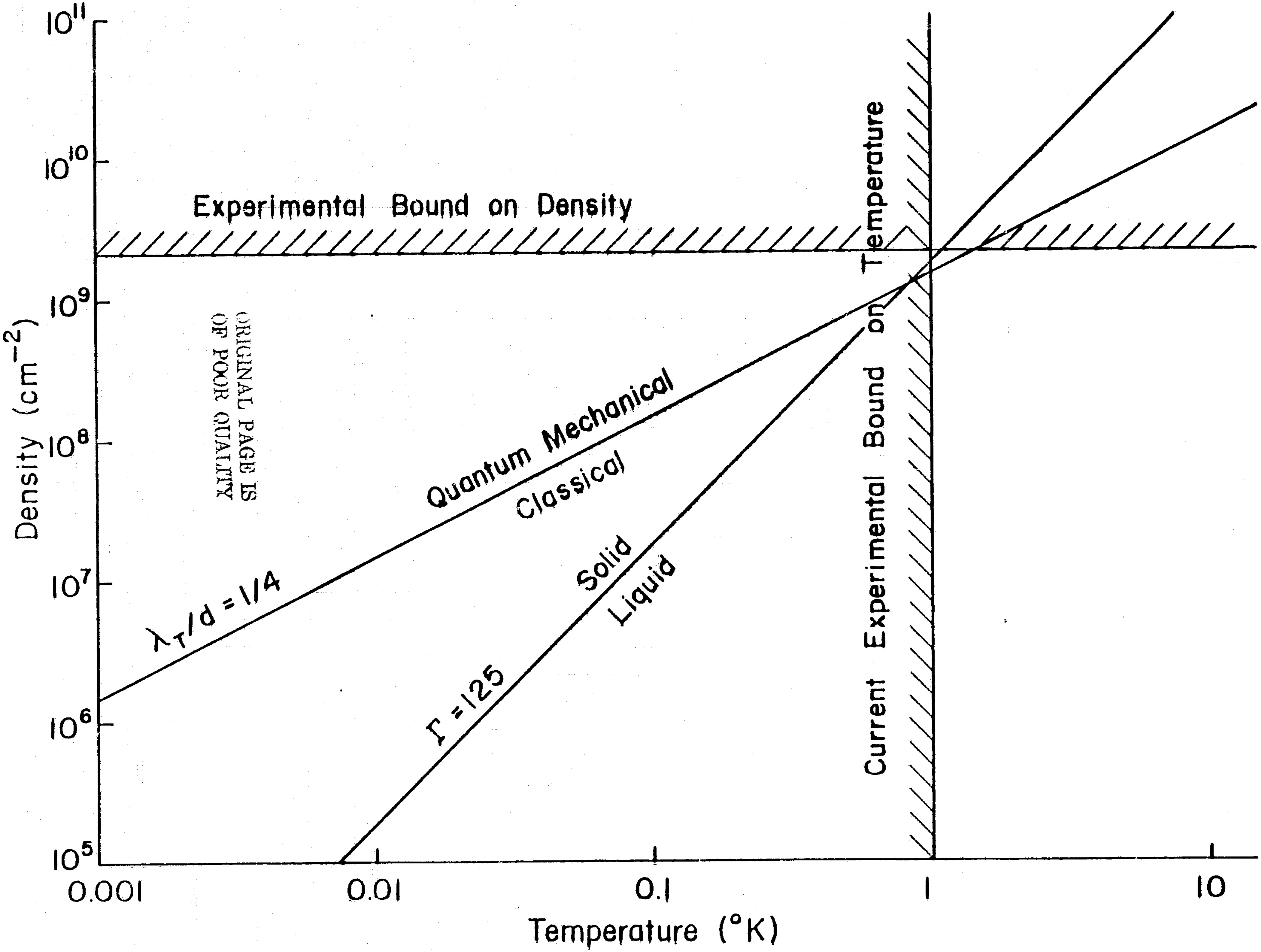

Experimental Bound on Density
Current Experimental Bound on Temperature
Quantum Mechanical
Classical
$\lambda_T/d = 1/4$
Solid
Liquid
$\Gamma = 125$
ORIGINAL PAGE IS OF POOR QUALITY
Density (cm$^{-2}$)
$10^{11}$
$10^{10}$
$10^{9}$
$10^{8}$
$10^{7}$
$10^{6}$
$10^{5}$
0.001
0.01
0.1
1
10
Temperature (°K)